Neurobiology of Disease 220 (2026) 107291

Contents lists available at ScienceDirect

Neurobiology of Disease

journal homepage: www.elsevier.com/locate/ynbdi

# GDF-11, GDF-15, Jag-1, and leptin in neuronal-derived extracellular vesicles as aging-related biomarkers to identify individuals at risk of Alzheimer's dementia: A pilot study

Simona Lanzillotta [a,1], Virginia Boccardi [b,1], Barbara Zulli [a], Alessandro Napoli [c], Gabriele Paolozzi [a], Roberta Angelini [d], Barbara Ruzicka [d], Federica Fratini [e], Anna Giulia Guazzarini [b,f], Michela Scamosci [b], Patrizia Bastiani [b], Martina Alunno [b], Eric Westman [f,g], Fabio Di Domenico [a], Marzia Perluigi [a], Antonella Tramutola [a], Roberta Cecchetti [b], Tommaso Mazza [c], D. Allan Butterfield [h], Patrizia Mecocci [b,f,**], Eugenio Barone [a,*]

[a] Department of Biochemical Sciences "A. Rossi-Fanelli", Sapienza University of Rome, Piazzale A. Moro 5, 00185 Rome, Italy
[b] Division of Gerontology and Geriatrics, Department of Medicine and Surgery, University of Perugia, Santa Maria della Misericordia Hospital, Piazzale Gambuli 1, 06132 Perugia, Italy
[c] Computational Biology and Bioinformatics UOS, Fondazione Policlinico Universitario Agostino Gemelli IRCCS, Largo Agostino Gemelli, 8, 00168 Roma, Italy
[d] Institute for Complex Systems National Research Council (ISC-CNR), Sede Sapienza, and Department of Physics, Sapienza University, Piazzale Aldo Moro, 00185 Rome, Italy
[e] Department of Neuroscience, Italian National Health Institute (ISS), Viale Regina Elena, 299, 00161 Rome, Italy
[f] Division of Clinical Geriatrics, Department of Neurobiology, Care Sciences and Society, Karolinska Institute, Stockholm, Sweden
[g] The Ageing Epidemiology Research Unit, School of Public Health, Imperial College London, London, UK
[h] Sanders-Brown Center On Aging, Department of Chemistry, University of Kentucky, 249 Chemistry-Physics Building, Lexington, KY 40506-0055, USA

## ARTICLE INFO

*Keywords:*
Aging
Alzheimer's disease
Biomarkers
Early diagnosis
Neuronal-derived extracellular vesicles
Sex differences

## ABSTRACT

Aging is the strongest risk factor for Alzheimer's disease (AD). Identifying reliable biomarkers of brain aging helps to predict functional decline and dementia onset. Evaluations of aging-related biomarkers in plasma and neuronal-derived extracellular vesicles (nEVs) from cognitively healthy and AD subjects, alongside post-mortem IPL brain samples from control (Ctr), pre-clinical AD (PCAD), mild cognitive impairment (MCI) and AD cases were performed. Cognitive tests, functional assessments, and MRI data were also included. Biomarkers in nEVs more accurately reflected brain pathology than those measured in plasma and showed stronger associations with cognitive and functional decline. Sex-specific patterns also emerged: GDF-15 was higher in nEVs from females with AD, whereas IL-6, IL-18 and Jag-1 were higher in nEVs from males with AD. A minimal nEV-derived panel including lower GDF-11 and higher GDF-15, Jag-1 and Leptin (after correction for age and sex) discriminated AD from Ctr and was associated with MRI-determined cortical atrophy in regions vulnerable to AD. These markers captured aging-related molecular trajectories that were disrupted in AD, and key associations observed in nEVs

*Abbreviations:* AD, Alzheimer's disease; ADL, Activities of Daily Living; APOA1, Apolipoprotein A1; Aβ, Amyloid-beta; CNS, Central nervous system; CTACK, Cutaneous T-cell–attracting chemokine; DLS, Dynamic light scattering; EVs, Extracellular vesicles; FGF-21, Fibroblast growth factor 21; GDF-11, Growth differentiation factor 11; GDF-15, Growth differentiation factor 15; GnRH, Gonadotropin-releasing hormone; HDL, High-density lipoprotein; IADL, Instrumental Activities of Daily Living; ICV, Intracranial volume; IL-6, Interleukin-6; IL-10, Interleukin-10; IL-18, Interleukin-18; IPL, Inferior parietal lobule; Jag-1, Jagged-1; LDL, Low-density lipoprotein; L1CAM, L1 cell adhesion molecule; MCI, Mild cognitive impairment; MISEV, Minimal Information for Studies of Extracellular Vesicles; MMSE, Mini-Mental State Examination; MTA, Medial temporal atrophy; MRI, Magnetic resonance imaging; NTA, Nanoparticle tracking analysis; PA, Posterior atrophy; PBS, Phosphate-buffered saline; PCAD, Preclinical Alzheimer's disease; SCP, Superficial cortical atrophy pattern; SIMCA, Soft Independent Modeling of Class Analogy; VES, Erythrocyte sedimentation rate; VIF, Variance inflation factor.

* Corresponding author at: Department of Biochemical Sciences "A. Rossi-Fanelli", Sapienza University of Rome, Piazzale A. Moro 5, 00185, Rome, Italy.
** Corresponding author at: Division of Gerontology and Geriatrics, Department of Medicine and Surgery, University of Perugia, Santa Maria della Misericordia Hospital, Piazzale Gambuli 1, 06132 Perugia, Italy.
*E-mail addresses:* patrizia.mecocci@unipg.it (P. Mecocci), eugenio.barone@uniroma1.it (E. Barone).
[1] Simona Lanzillotta and Virginia Boccardi equally contributed to this work.

https://doi.org/10.1016/j.nbd.2026.107291
Received 13 October 2025; Received in revised form 27 December 2025; Accepted 26 January 2026
Available online 28 January 2026

were confirmed in post-mortem brain tissue. Our results suggests that nEV-derived biomarkers capture early, brain-specific and sex-modulated aging signatures, providing superior sensitivity compared to plasma. Their convergence with post-mortem findings underscores their biological validity and translational potential. These results highlight the value of nEVs for stratifying individuals at higher risk of AD and support their integration into precision medicine approaches for dementia prevention.

## 1. Background

Aging is the most significant risk factor for Alzheimer's disease (AD), the most frequent form of neurodegenerative dementia (Zhang et al., 2024). As global life expectancy increases, the prevalence of AD is projected to rise, presenting a growing public health challenge (Zhang et al., 2024). The AD continuum spans from preclinical stages, through mild cognitive impairment (MCI), to overt dementia. Beyond many theories AD is characterized by progressive cognitive decline, memory impairment, and synaptic dysfunction, and from a neuropathological point of view by amyloid-beta (Aβ) plaques deposition and tau hyperphosphorylation, as well as neuroinflammation, insulin resistance and oxidative stress (Zhang et al., 2024; Perluigi et al., 2024; Triani et al., 2018; Tramutola et al., 2018; Barone and Butterfield, 2025). The aging brain undergoes biological changes, including insulin resistance, elevated oxidative stress, mitochondrial dysfunction, impaired proteostasis, and chronic low-grade inflammation collectively referred to as "inflammaging" (Franceschi et al., 2018). These alterations compromise neuronal integrity and communication, thereby creating a vulnerable milieu that predisposes the brain to neurodegenerative processes (Franceschi et al., 2018). Notably, this chronic inflammatory state is not confined to the central nervous system (CNS) but reflects a bidirectional crosstalk between the brain and peripheral systems (Tian et al., 2012), whereby systemic inflammatory signals influence neural homeostasis and, conversely, brain-derived factors modulate peripheral immune and metabolic responses (Muller and Di Benedetto, 2025).

Recent evidence has highlighted the role of extracellular vesicles (EVs), particularly neuron-derived extracellular vesicles (nEVs), as important mediators of intercellular communication within the CNS (Manolopoulos et al., 2025). nEVs carry proteins, lipids, and nucleic acids reflective of the physiological state of their neuronal origin and have been implicated in the propagation of pathological molecules such as Aβ, tau, and inflammatory mediators across the brain (Manolopoulos et al., 2025). Due to their ability to cross the blood-brain barrier and their detectability in peripheral biofluids, nEVs might be used as a liquid biopsy, since they offer a promising non-invasive approach for monitoring molecular changes associated with AD (Kapogiannis et al., 2019). Compared to plasma, nEVs show stronger associations with cognitive decline, brain atrophy, and clinical outcomes, and have demonstrated predictive value for conversion from MCI to AD (Manolopoulos et al., 2023).

Despite these advances, several key gaps remain: the mechanistic role of nEVs in AD pathogenesis is still unclear; age-related dynamics of nEVs are poorly characterized; and sex-specific differences remain largely unexplored. Furthermore, few studies have assessed comprehensive biomarker panels that integrate inflammatory, metabolic, and neuroprotective signals in relation to brain aging and AD (Manolopoulos et al., 2025).

The selection of the biomarkers was guided by their complementary involvement in the core biological axes implicated in brain aging and AD, namely metabolic dysfunction, systemic and neuroinflammatory activation, as well as cellular senescence. Metabolic regulators such as Growth Differentiation Factor 11 (GDF-11), Growth Differentiation Factor 15 (GDF-15), leptin and Fibroblast Growth Factor 21 (FGF-21) have been repeatedly associated with impaired energy sensing, mitochondrial stress responses, and neuro-metabolic coupling, processes known to deteriorate early in AD (Jena et al., 2023; Liu et al., 2021; Wang et al., 2023; Nakamichi et al., 2025; Kapoor and Nation, 2021; Charisis et al., 2024). In parallel, inflammatory cytokines including IL-6, IL-10, and IL-18, together with chemokines such as Cutaneous T-Cell–Attracting Chemokine (CTACK, also known as CCL27), capture distinct aspects of the peripheral and central immune milieu, reflecting microglial activation, cytokine drift, and chronic low-grade inflammation that accelerate neurodegenerative cascades (Jena et al., 2023; Liu et al., 2021; Wang et al., 2023; Nakamichi et al., 2025; Kapoor and Nation, 2021; Charisis et al., 2024). Neuroendocrine factors such as Gonadotropin-Releasing Hormone (GnRH) and the Notch-pathway ligand Jagged-1 (Jag-1) were also included (Jena et al., 2023; Liu et al., 2021; Wang et al., 2023; Nakamichi et al., 2025; Kapoor and Nation, 2021; Charisis et al., 2024). This integrated panel therefore includes converging pathways that collectively shape the trajectory of brain aging. Nevertheless, when quantified in whole plasma, these markers provide only an indirect proxy of CNS-specific alterations. nEVs, by isolating vesicles of neuronal origin, offer a more precise window into these aging-related molecular signatures and improve the interpretability of the biomarker panel within a brain-specific context (Manolopoulos et al., 2025).

In this pilot study, we profiled a panel of aging- and metabolism-related markers in both plasma and L1CAM-enriched nEVs from cognitively intact and AD individuals. To strengthen the biological relevance of peripheral biomarkers, we complemented our analyses with a validation step in post-mortem brain tissue. We measured the same panel of markers in inferior parietal lobule (IPL) samples from an independent cohort of well-characterized donors across the AD continuum. Although these brain samples were derived from individuals distinct from those included in the plasma and nEVs analyses, this parallel approach enabled us to assess the degree of concordance between circulating and brain-derived molecular signatures of aging and neurodegeneration. Our goal was to determine whether nEVs offer superior reflection of brain pathology compared to plasma, and to explore how age, sex, and clinical status modulate these biomarkers.

## 2. Methods

### 2.1. Study participants

For the present study, we enrolled a total of 28 subjects (16 F/12 M) divided into two groups – AD subjects ($n$ = 14) and age-matched cognitively healthy controls (Ctr, n = 14) – from the GeriCo study (Geriatric Cognitive Evaluation, https://gericoev.eu). This is a clinical and biological based project at the division of Gerontology and Geriatrics, University of Perugia, focused on cognitive impairment and dementia in older adults. The general inclusion criteria were as follows:

#### 2.1.1. Cognitively healthy controls

Age and education adjusted MMSE score $\geq$ 27; no active neurological or psychiatric disorders; no ongoing medical problems or related treatments interfering with cognitive functions; a normal neurological exam; no psychoactive medications; the ability to live and function independently in the community.

#### 2.1.2. Alzheimer's dementia

Dementia was diagnosed according to standard research criteria (McKhann et al., 2011) by a combination of clinical and neuropsychological evaluation and brain imaging. The severity of the disease was mild to moderate (clinical dementia rating scores 1 and 2).

Participants recruited provided informed consent, and the study adhered to the Declaration of Helsinki and was approved by the Regional Ethical Committee (Prot. N. CE-1065/24 del 24/07/2024). Consent for inclusion in the study was obtained during a visit to outpatient clinics from all participants and was archived for participation/publication.

### 2.2. Multidimensional and cognitive performance assessment

Clinical information was obtained by history and multidimensional evaluation. Expert neuropsychologists assessed participants through an extended neuropsychological battery, as previously reported (Boccardi et al., 2024). The Mini-Mental State Examination was used as a screening test (Folstein et al., 1975). A score $\geq$ 27/30 is generally considered to indicate normal cognitive function in most individuals. Functional status was assessed using informant-based evaluations through two standardized instruments: the Activity of Daily Living (ADL) scale and the Instrumental Activity of Daily Living (IADL) scale (Katz et al., 1963; Lawton and Brody, 1969). The ADL scale measured basic self-care tasks such as bathing, dressing, toileting, transferring, continence, and feeding, whereas the IADL scale evaluated more complex activities necessary for independent living, including telephone use, medication management, shopping, food preparation, housekeeping, laundry, transportation, and financial handling. Informants were instructed to report on the patient's current level of independence, with scores assigned according to established scoring criteria. Assessments were conducted in a standardized format by trained personnel to ensure inter-rater consistency.

### 2.3. Clinical and biochemical variables assessment

All participants underwent a clinical work-up. Blood samples were collected in the morning after fasting overnight, measuring fasting glycaemia (mg/dl), azotemia (mg/dl), VES, PCR (mg/dl), creatininemia (mg/dl), creatinine clearance (ml/min), uric acid (mg/dl), total cholesterol (mg/dl), high-density lipoprotein cholesterol (HDL, mg/dL), triglycerides (mg/dL), low-density lipoprotein cholesterol (LDL, mg/dL), vitamin B12 (pg/ml), folic acid (ng/ml) by standard laboratory methods (Supplementary Table 1).

### 2.4. Magnetic resonance imaging (MRI)

Magnetic resonance imaging was performed using a standard 3.0 Tesla system (Signa Advantage, GE Medical Systems, Milwaukee, WI, USA) according to the ADNI protocol (Jack Jr. et al., 2024). Patients were positioned supine with head immobilization to minimize motion artifacts. Conventional MRI sequences included T1-weighted, T2-weighted, and fluid-attenuated inversion recovery (FLAIR) images acquired in axial, sagittal, and coronal planes. Image acquisition parameters (e.g., slice thickness, repetition time, echo time) were standardized across all scans. High-resolution T1-weighted MRI scans (1 $mm^3$ isotropic) from each participant were processed using FreeSurfer's standard recon-all pipeline (v6.0) through the TheHiveDB system (Muehlboeck et al., 2014). This included skull stripping, tissue segmentation, and surface reconstruction to produce volumetric outputs. From these processed scans, we extracted regional measures of cortical thickness, surface area, and subcortical/cortical volumes based on the Desikan-Killiany atlas (FreeSurfer v6.0). Volumetric measures were normalized by total intracranial volume (ICV) to account for inter-individual differences in head size. In addition to these quantitative measures, visual assessment of brain atrophy was performed using validated clinical rating scales, including medial temporal atrophy (MTA), posterior atrophy (PA), and superficial cortical atrophy pattern (SCP) scores. These regional and visual metrics were subsequently used for the correlation and clustering analyses described in the Results section. All images were independently reviewed by two experienced neuroradiologists blinded to the clinical data.

### 2.5. Plasma samples collection

Blood samples were obtained from all participants after overnight fasting. All blood draws and processing followed established protocols using standard venipuncture procedures. Blood was collected in ethylenediaminetetraacetic acid (EDTA) polypropylene tubes and was centrifuged at 850 $\times g$ for 15 min at 4 °C. Afterward, plasma was isolated and centrifuged again at 850 $\times g$ for 15 min at 4 °C to eliminate clots and aggregates. Plasma samples were then divided into 0.5-mL aliquots and stored at −80 °C until analysis. Preanalytical factors for blood collection and storage complied with international guidelines for EVs biomarkers (Welsh et al., 2024).

### 2.6. nEVs isolation

nEVs isolation was performed as previously described by our group (Perluigi et al., 2022). Plasma samples were thawed on ice and defibrinated with thrombin (System Biosciences, Inc., Mountain View, CA) followed by 30 min incubation at room temperature. Two-hundred fifty µL of plasma were diluted 1:1 *v*/v with Dulbecco's calcium and magnesium-free salt solution (DSB, Thermo Scientific, Inc., Waltham, MA) with addition of protease (#P8340, Sigma–Aldrich, St Louis, MO, USA) and phosphatase inhibitors (#P5726, Sigma–Aldrich, St Louis, MO, USA). Total EVs were collected using an Exo-spin Blood kit EX-02™ (Cell Guidance, Cambridge, UK) according to the manufacturer's instructions and finally resuspended in 0.5 mL of ultra-pure distilled water with the manufacturer-recommended concentration of protease and phosphatase inhibitors. To immunocapture L1 Cell Adhesion Molecule (L1CAM)-positive nEVs, the suspension was incubated for 1 h at 4 °C with 4 µg of mouse anti-human CD171 (L1CAM) biotinylated antibody (clone 5G3) (Thermo Scientific, Inc.), followed by incubation with 25 µL of Pierce™ Streptavidin Plus UltraLink™ Resin (Thermo Scientific, Inc.) for 30 min at 4 °C. After centrifugation at 800 $\times g$ for 10 min at 4 °C and removal of supernatant, nEVs were eluted with 200 µL of 0.1 M glycine. Beads were then sedimented by centrifugation at 4500 $\times g$ for 5 min at 4 °C and the supernatants containing nEVs were transferred to clean tubes. pH was neutralized with 1 M Tris-HCl, and samples underwent 2 freeze/thaw cycles with M-PER™ protein extraction reagent (Thermo Scientific, Inc.) supplemented with protease and phosphatase inhibitors. The final suspensions containing nEVs proteins were stored at −80 °C. Samples were thawed and vortexed twice prior to protein measurements. The stored suspensions were used to determine the total protein concentration by the Bradford assay (Pierce, Rockford, IL). All investigators involved in nEVs isolation and biomarker quantification were blinded until all measurements were completed.

### 2.7. nEVs characterization by dynamic light scattering (DLS) and nanoparticle tracking analysis (NTA)

The hydrodynamic radius, $R_H$, of the particles isolated from each sample was determined through Dynamic Light Scattering (DLS). Measurements were carried out at 25 °C on 10 µL dilute suspensions (1:100) with an optical setup employing a solid-state laser emitting a monochromatic and polarized beam at a wavelength of $\lambda = 642$ nm. Data were collected at a fixed scattering angle of $\theta = 90°$, corresponding to a scattering vector $Q = 4\pi n/\lambda \sin(\theta/2) = 0.018\ nm^{-1}$, where $n = 1.33$ is the refractive index of water, the solvent used. The hydrodynamic radius was calculated using the Stokes-Einstein equation:

$$R_H = k_B T/6\pi\eta D$$

here, $k_B$ is the Boltzmann constant, $\eta$ is the viscosity of water at the measured temperature, and D is the translational diffusion coefficient. The diffusion coefficient was extracted from the relaxation time $\tau$, using

the relation:

$$D = 1/Q^2\tau$$

The relaxation time was obtained by fitting the intensity autocorrelation function using the Kohlrausch-Williams-Watts (KWW) stretched exponential model:

$$g_2(Q,t) = 1 + b\left[\exp\left(-(t/\tau)^{\beta}\right)\right]^2$$

where the stretching exponent β characterizes deviations from a single exponential decay. In addition, NanoSight NS300 (Malvern Panalytical, Ltd., Malvern, UK) was also used for NTA to measure size and concentration of a blind subgroup of nEVs ($n = 10$), in accordance with commonly adopted procedures in the field, where representative sample subsets are routinely analyzed to confirm particle size distribution and concentration profiles (Ledreux et al., 2025; Kapogiannis et al., 2024). To get a suitable concentration, the samples were diluted 1:40 in particle-free PBS (0.02 mm filtered). The instruments were equipped with a 488 nm laser (blue), a high-sensitivity sCMOS camera, and a syringe pump that flowed the sample at a speed of 30 arbitrary units (that indicates the relative speed at which the syringe pump is dispensing the sample). Five videos, each 60 s long, were acquired for each sample at a camera level of 15 under automated script control and analysis was conducted using NTA 3.4 Build 3.4.4 software setting, the detection threshold at 5 and the other parameters were kept as default.

### 2.8. nEVs characterization for EVs and neuronal biomarkers

The detection of both transmembrane and intravesicular EV markers is required to confirm the sequential enrichment of EVs from neat plasma. EVs enrichment was confirmed on a subgroup of samples randomly chosen ($n = 13$: CTR $n = 6$ and AD $n = 7$) as previously done in larger studies (Ledreux et al., 2025; Kapogiannis et al., 2024) by showing the presence of transmembrane (cluster of differentiation 81, CD81) and intravesicular EV markers (Alix) in both total EVs, non-neuronal EVs and nEVs. Relative depletion of lipoprotein (Apolipoprotein-A1, APOA1) and Golgi marker GM130 was also tested in nEVs. Moreover, enrichment of EVs of neuronal origin was confirmed by evaluating L1CAM levels, as neuronal markers (Nogueras-Ortiz et al., 2024). The evaluation of the markers mentioned above was performed by Western blot analysis described below.

### 2.9. Western blot analysis

Five μg of proteins for each sample were resolved on Criterion TGX Stain-Free 4–15% 18-well gel (Bio-Rad Laboratories, Hercules, CA, USA; #5678084) in a Criterion large format electrophoresis cell (Bio-Rad Laboratories, #1656001) in Tris/Glycine/SDS (TGS) running buffer (Bio-Rad Laboratories, #1610772). Afterward, the gel was placed on a Chemi/UV/Stain-Free tray and visualized using a ChemiDoc MP imaging System (Bio-Rad Laboratories, #17001402) in UV setting. Total protein load was assessed using the Image Lab Software (Bio-Rad Laboratories). Subsequently, proteins were transferred via a TransBlot Turbo semi-dry blotting apparatus (Bio-Rad Laboratories, #1704150) onto nitrocellulose membranes (Bio-Rad Laboratories, #162–0115). Membranes were blocked with 3% bovine serum albumin in 0.5% Tween-20/Tris-buffered saline (TBS-t) and incubated overnight at 4 °C with the following antibodies: anti-CD81 (1:1000, Thermo Scientific, Inc., #MA5–32333), anti-Alix (1:500, Santa-Cruz, #SC-47701), anti-L1CAM (1:1000, Cell Signaling, #89861S), anti-APOA1 (1:1000, Thermo Scientific, Inc., #MA5–514668), anti-GM130 (1:100, Abcam, #Ab52649). For L1CAM detection, an antibody targeting the C-terminal region of the protein was used, while nEVs were immunoprecipitated with an antibody targeting the N-terminal region (5G3). After 3 washes with TBS-t buffer, membranes were incubated for 60 min at room temperature with appropriate secondary antibodies conjugated with horseradish peroxidase (1:5000; Sigma–Aldrich, St. Louis, MO, USA). Membranes were developed with Clarity enhanced chemiluminescence (ECL) substrate (Bio-Rad Laboratories, #1705061), the signal was acquired with Chemi-Doc MP (Bio-Rad Laboratories) and analyzed using Image Lab software (Bio-Rad Laboratories). Normalization was performed against the total proteins load signal.

### 2.10. Post-mortem brain samples

Brain tissues from well-characterized subjects were obtained from an independent cohort of samples and provided by the Sanders-Brown Center on Aging at the University of Kentucky. Analyses were performed on the inferior parietal lobule (IPL) of preclinical AD (PCAD), amnestic MCI, AD cases and age-matched Ctrs. Clinical diagnosis of disease stage was made as described previously (Aluise et al., 2010; Aluise et al., 2011). Age and gender are listed in the Supplementary Table 2. The short post-mortem interval range was between 2 and 4 h and was comparable between the three groups. The degree of cognitive impairment was assessed using the Mini Mental State Examination (MMSE) (and listed in Supplementary Table 2). Total protein extracts were prepared in RIPA buffer (pH = 7.4) containing 50 mM Tris-HCl (pH = 8), 150 mM NaCl, 1% NP-40, 0.5% sodium deoxycholate,1 mM EDTA, 0.1% SDS, together with phosphatase and protease inhibitor (539,132, Millipore, 1:100; P0044; Sigma-Aldrich, St. Louis, MO, USA; 1:100). Samples were sonicated on ice and then centrifuged at 14.000 rpm at 4 °C for 30 min to remove cellular debris. Supernatants were collected to determine total protein concentrations by the BCA method (Pierce, Rockford, IL, USA).

### 2.11. Multiplex assay

A multiplex biometric ELISA-based immunoassay was used according to the manufacturer's instructions (MILLIPLEX® Human Aging Magnetic Bead Panel 1 - Metabolism Multiplex Assay, Millipore, Burlington, MA, USA) to evaluate CTACK, FGF-21, GDF-11, GDF-15, GnRH, IL-10, IL-18, IL-6, Jag-1, and Leptin levels in nEVs, plasma, and post-mortem brain samples. Measurements were performed in duplicate. The analyte concentration was calculated using a standard curve, as provided by the manufacturer's software (Bio-Plex Manager Software, version 5, Bio-Rad Laboratories, Hercules, CA, USA). For nEVs and post-mortem brain samples, the concentration of each marker was calculated as a ratio between the measured amount and the total proteins loaded.

### 2.12. Statistical analyses

Data distributions were assessed for normality using the Shapiro–Wilk test and by visual inspection where appropriate. Depending on the distributional properties of each variable and analysis, either parametric or non-parametric methods were applied. For comparisons between two independent groups, the two-tailed Mann–Whitney *U* test was used when normality assumptions were not met; otherwise, the appropriate parametric test was applied. For comparisons involving more than two groups, the Kruskal–Wallis test followed by Dunn's post hoc test was used for non-normally distributed variables, whereas one-way ANOVA with appropriate post hoc testing was used when assumptions were satisfied. Unless otherwise specified, $p < 0.05$ was considered statistically significant. Data visualization included boxplots to display biomarker distributions across diagnostic groups (AD vs Ctr), stratified by sex. Correlation analyses were intended to explore associations and concordance patterns rather than to build explanatory linear models. Therefore, associations between continuous variables were evaluated using Pearson's correlation coefficients. For each correlation matrix, multiple comparisons were controlled within that family of tests using the Benjamini–Hochberg false discovery rate (FDR) procedure. For all tests, we reported *p*-values of correlations that survived after FDR correction. Adjusted q-values <0.05 were considered statistically

significant. For assessing similarities between biomarker profiles in plasma, nEVs, and post-mortem brain tissue, Spearman's rank correlation coefficients (ρ) were calculated on average biomarker levels within each group. This analysis was conducted separately for AD and Ctr subjects. For each group, the mean abundance of each biomarker in the three compartments was calculated, and ranked profiles were compared to assess the degree of concordance between nEVs and the brain, and between plasma and the brain. To explore similarities among brain regions based on their correlation profiles with aging-related biomarkers, we performed hierarchical clustering on the matrix of significant Pearson correlation coefficients ($p$-value $<0.05$). Correlation matrices were computed separately for biomarkers measured in nEVs and plasma, and for two categories of brain imaging features: (Zhang et al., 2024) conventional MRI-derived structural metrics, and (Perluigi et al., 2024) clinically derived visual rating scales or composite scores, described above. Each correlation matrix was arranged with brain regions as rows and biomarkers as columns, and only statistically significant values were retained. The resulting matrices were then clustered using agglomerative hierarchical clustering with average linkage and Euclidean distance as the similarity metric. Cluster heatmaps were generated using the *clustermap* function from the seaborn Python library, with dendrograms displayed along both axes and annotations shown only for non-zero correlations. Color coding ranged from red (positive) to blue (negative) to reflect the strength and direction of each correlation. To investigate patterns in biomarker distribution, we employed dimensionality reduction and clustering techniques. Principal Component Analysis (PCA) was applied to the standardized dataset of nEV biomarkers, retaining the first three components for 3D visualization. To assess whether the selected biomarkers naturally grouped AD and CTR subjects into distinct clusters, we applied the K-means method, setting the number of clusters to 2 and a fixed random seed to ensure reproducibility. Clustering performance was evaluated using the silhouette score. To further explore associations between biomarkers and diagnosis, logistic regression models were fitted using the Logit function from statsmodels. Predictors included the nEV biomarkers, as well as covariates such as age and sex (encoded as binary). The predictive performance of the models was assessed using the area under the receiver operating characteristic curve (ROC-AUC). Predictor importance was assessed using Random Forest feature importance scores, and redundancy among predictors was evaluated using multicollinearity diagnostics via the Variance Inflation Factor (VIF). To evaluate the discriminative power of selected biomarkers between AD and Ctr samples, a SIMCA (Soft Independent Modeling of Class Analogy) approach was applied based on principal component analysis (PCA). Results were visualized using 3D scatter plots of PCA scores, created with the mpl_toolkits.mplot3d library. In 3D visualizations, the $T^2$ threshold was rendered as a reference ellipsoid to facilitate interpretation. All statistical analyses were conducted using Python (version 3.10.4), leveraging SciPy (1.10.1), scikit-learn (1.2.2), statsmodels (0.13.2), seaborn (0.11.2), and matplotlib (3.5.3).

## 3. Results

### 3.1. Characterization of nEVs

nEVs preparations were characterized for size and protein content, along with immunoblotting analyses for positive and negative EVs markers, according to established criteria (Welsh et al., 2024) (Fig. 1A). The size distribution of nEVs immunocaptured by L1CAM was studied using DLS (Fig. 1B and C). Furthermore, NTA revealed an enrichment of nEVs in the expected size range consistent with DLS measures (Fig. 1D and Supplementary Fig. 1). The correlation coefficients of nEVs from both participant groups were consistent with EVs guidelines (Welsh et al., 2024), as were the mean hydrodynamic diameter values (105 ± 10.6 nm and 125 ± 11 nm, in Ctr and AD, respectively) (Fig. 1E). The size of nEVs was comparable between the groups (Fig. 1E). The quantification of nEVs was performed by measuring the total protein content by Bradford assay, which provides an estimation of the amount of nEVs (Thery et al., 2018; Gauthier et al., 2017). Similar nEVs levels were observed between the Ctr and AD groups (Fig. 1F). The purification of nEVs was confirmed by western blot analysis, which showed enrichment of transmembrane and intravesicular EV markers, i.e., CD81 and Alix (Fig. 1G), and relative depletion of lipoprotein, i.e., APOA1, and the Golgi marker GM130 in nEVs (Fig. 1H). A significant increase in L1CAM levels in nEVs compared with total EVs both for CD81(nEVs/total EVs = 7.04) and Alix (nEVs/total EVs = 6.6), confirmed the enrichment of nEVs by L1CAM immunoprecipitation (Fig. 1G, I and J). The degree of neuronal enrichment is consistent with previous studies reporting enrichment values from 1.6-fold to 5.6-fold, depending on the marker (Mustapic et al., 2017). In addition, the evaluation of the eluate (non-neuronal EVs) from the L1CAM immunocapture of nEVs further reveals that nEVs are enriched in L1CAM, while EV markers CD81 and Alix can be observed in both nEVs and non-neuronal EVs (Fig. 1G).

### 3.2. nEVs markers of aging levels in the nEVs, plasma and post-mortem brain samples

Aging biomarkers were measured in nEVs and plasma obtained from the same individuals enrolled in this study, and in an independent cohort of postmortem brain samples from Ctr and AD subjects. For nEVs and postmortem brain tissue, marker levels were expressed relative to the total amount of protein loaded in the assay, whereas plasma concentrations were reported per mL of sample. For nEVs, the total protein used for normalization corresponds to Bradford quantification of the L1CAM-immunocapture eluate. We adopted a protein-based normalization for nEV analyses to ensure that biomarker measurements were compared across equivalent amounts of immunocaptured nEV-derived material (Thery et al., 2018; Gauthier et al., 2017).

The analysis of aging markers in the nEVs did not reveal any significant differences between Ctr and AD subjects (Fig. 2A-J), nor were any differences found in the plasma samples (Fig. 2K-T). Notably, for specific biomarkers (e.g., GDF-11, GnRH, and Jag-1), the evaluation in plasma samples was unsuccessful, because their signals were consistently below the lower limit of detection, most likely reflecting very low circulating concentrations in the plasma. By contrast, the same analytes were robustly detectable in nEVs, indicating that vesicle enrichment increases their measurable signal and provides a more reliable compartment for their assessment. To determine whether plasma biomarker levels might predict nEVs levels, we performed linear regression analyses for all biomarkers whose measurements were consistent in both nEVs and plasma samples (Supplementary Fig. 2). Our results showed significant associations for GDF-15 ($p = 0.0004$), Supplementary Fig. 2C) and Leptin ($p = 0.0016$, Supplementary Fig. 2G). Furthermore, to assess whether the measures performed in nEVs mirror brain alterations, we performed the same analyses in IPL post-mortem samples from an independent cohort of well-characterized donors across the AD continuum (age-matched Ctr, PCAD, MCI and AD subjects, Fig. 3). These samples were obtained from an independent group of subjects of similar age and outcomes in cognitive decline tests (i.e., MMSE) to those enrolled in the study testing nEVs (Supplementary Table 1). The IPL is a key region implicated in AD pathology and aging-related cognitive deterioration owing to its role in higher cognitive processes, such as attention, memory, and language (Wen et al., 2025a; Keith et al., 2024). The use of post-mortem IPL samples enables the direct assessment of molecular and cellular biomarkers of aging and neurodegeneration, providing crucial insights into the mechanisms underlying AD-related changes at the tissue level, which are otherwise difficult to study in vivo. Our results showed no significant differences among these groups (Fig. 3A-J), consistent with the results obtained for nEVs.

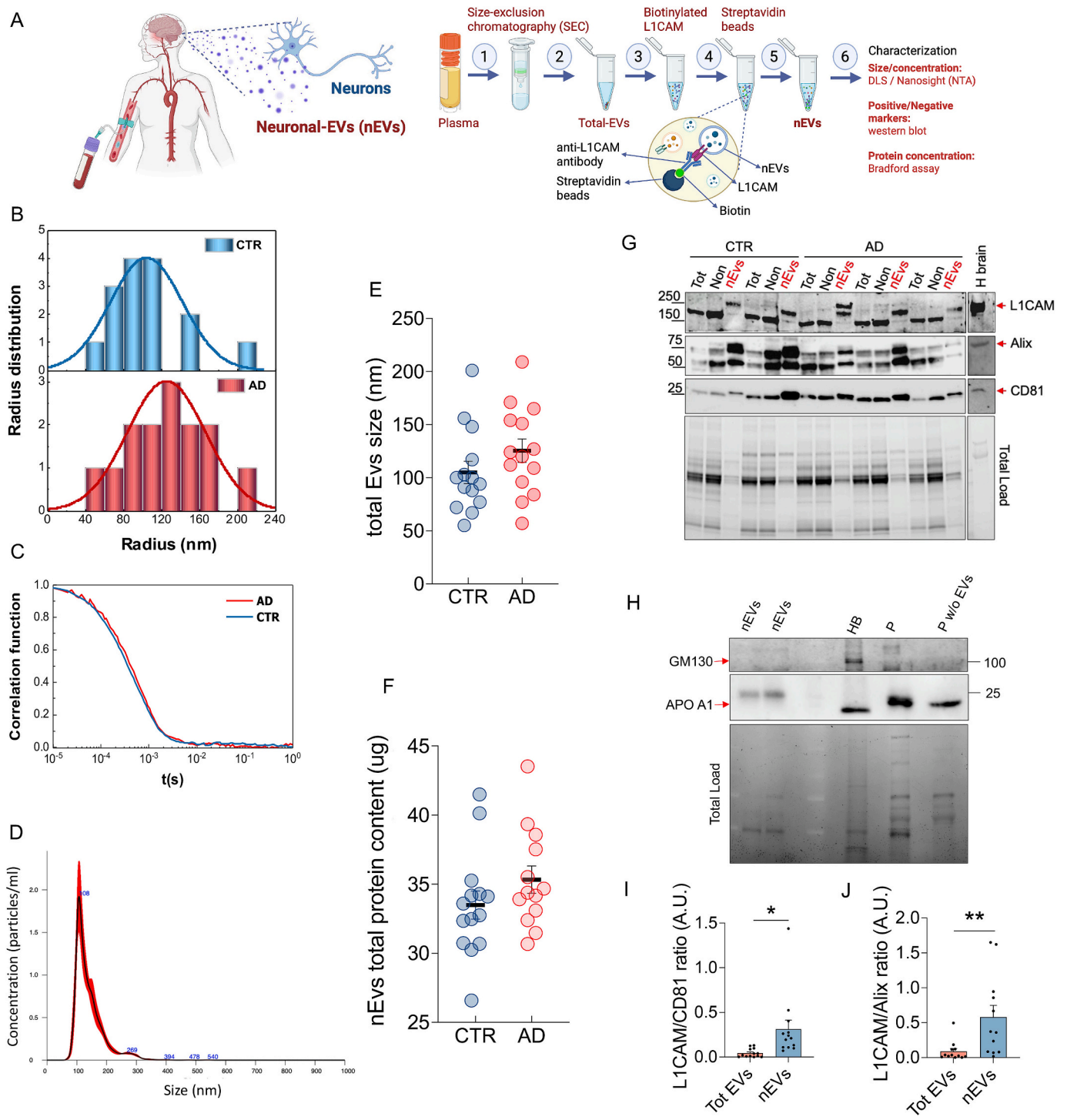


**Fig. 1.** Characterization of neuronal-derived extracellular vesicles (nEVs). (A) Schematic of the isolation and enrichment procedure for L1CAM+ nEVs from plasma. For all EV characterization, we adhered to the Minimal Information for Studies of Extracellular Vesicles (MISEV) 2023 guidelines. In (B) Size distribution and (C) correlation curve of nEVs from control (CTR, $n = 14$) and AD subjects (n = 14). (D) Representative nanoparticle tracking analysis (NTA) curve from a blind subgroup of samples ($n = 10$) showing mean size and concentration of nEVs. (E) Hydrodynamic diameter of nEVs isolated from CTR (n = 14) and AD subjects (n = 14) assessed by dynamic light scattering (DLS). (F) Total protein concentration of nEVs isolated from CTR (n = 14) and AD subjects (n = 14). (G-H) Representative Western blot images from a subset of samples ($n = 13$) showing the enrichment of neuronal (L1CAM) and EV-specific (CD81, Alix) markers and depletion of contaminants (APOA1, GM130). (I) and (J) Densitometric quantification of western blot confirming the neuronal enrichment (L1CAM/CD81 and L1CAM/Alix ratios) (n = 13). Tot: total EVs; Non: nEVs-depleted EVs; nEVs: neuronal-derived EVs; H: human brain homogenate; P: plasma; P w/o EVs: EV-depleted plasma. Data are shown as mean ± SEM. *$p < 0.05$ versus Total EVs (Unpaired *t*-test).

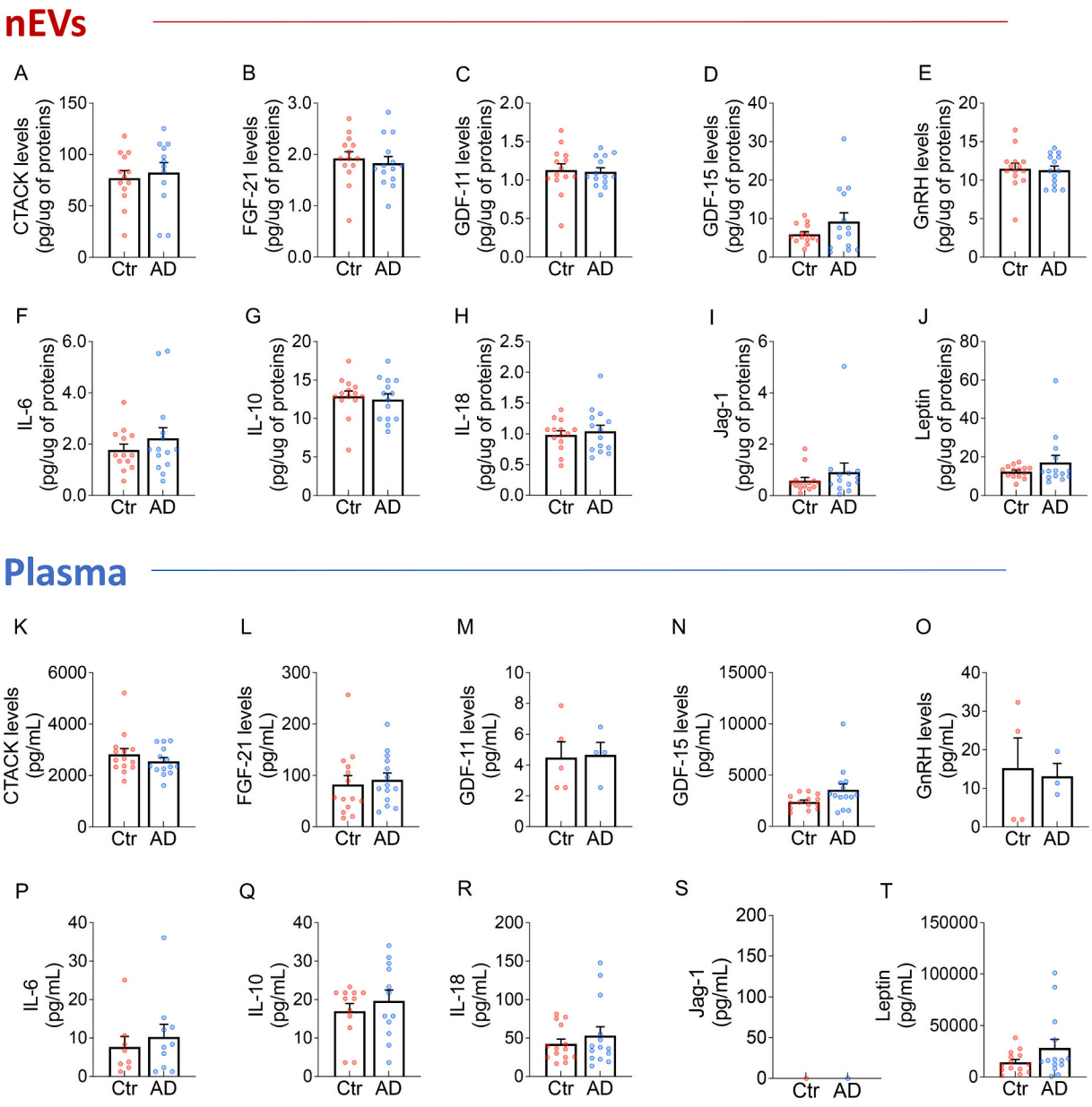


**Fig. 2.** Aging-related biomarker levels in nEVs and plasma from AD and control subjects. Levels of biomarkers measured in nEVs (A–J) and plasma (K–T) from AD (n = 14) and age-matched CTR subjects (n = 14). Data are presented as mean ± SEM. Group differences (AD vs CTR) were assessed using Unpaired *t*-tests for normally distributed variables and Mann–Whitney *U* tests otherwise. Data show no significant differences.

### *3.3. Changes of nEVs markers reflect changes observed in post-mortem brain samples*

To test whether the nEVs biomarkers' profile more closely reflected brain molecular alterations than those measured in plasma, we constructed a graph showing the average levels of each marker across three compartments – nEVs, plasma, and post-mortem brain IPL samples – in both Ctr and AD subjects. As shown in Fig. 3K–L, the overall distribution patterns of biomarkers in nEVs were more like those observed in brain tissue than those in plasma. To quantify this similarity, we calculated *Spearman correlation* coefficients between the ranked abundance profiles of the overall biomarkers in each compartment. In Ctr subjects, the correlation between nEVs and brain tissue was strong ($\rho = 0.782$), while the plasma–brain correlation was substantially lower ($\rho = 0.491$). A similar pattern emerged in AD subjects, with a higher nEVs–brain correlation ($\rho = 0.685$) compared to plasma–brain ($\rho = 0.430$). These findings indicate that the relative biomarker abundance measured in nEVs more faithfully captures the molecular profile of the aging brain than plasma measurements, in both healthy and disease conditions.

These results reinforce the idea that, for most of these biomarkers, evaluation in nEVs better reflects brain molecular alterations, positioning nEVs as a biologically meaningful source for tracking neurodegenerative processes.

### *3.4. Age-by-diagnosis interaction models uncover hidden differences in biomarker profiles*

One possible explanation for the lack of substantial differences between the Ctr and AD group is the advanced age of the participants, which may mask pathology-driven effects. Supporting this hypothesis, the Soft Independent Modeling of Class Analogy (SIMCA) analysis did not provide sufficient discriminatory power to accurately classify Ctr and AD subjects (Supplementary Fig. 3). To explore this further, we applied a linear mixed model to assess whether the differences between

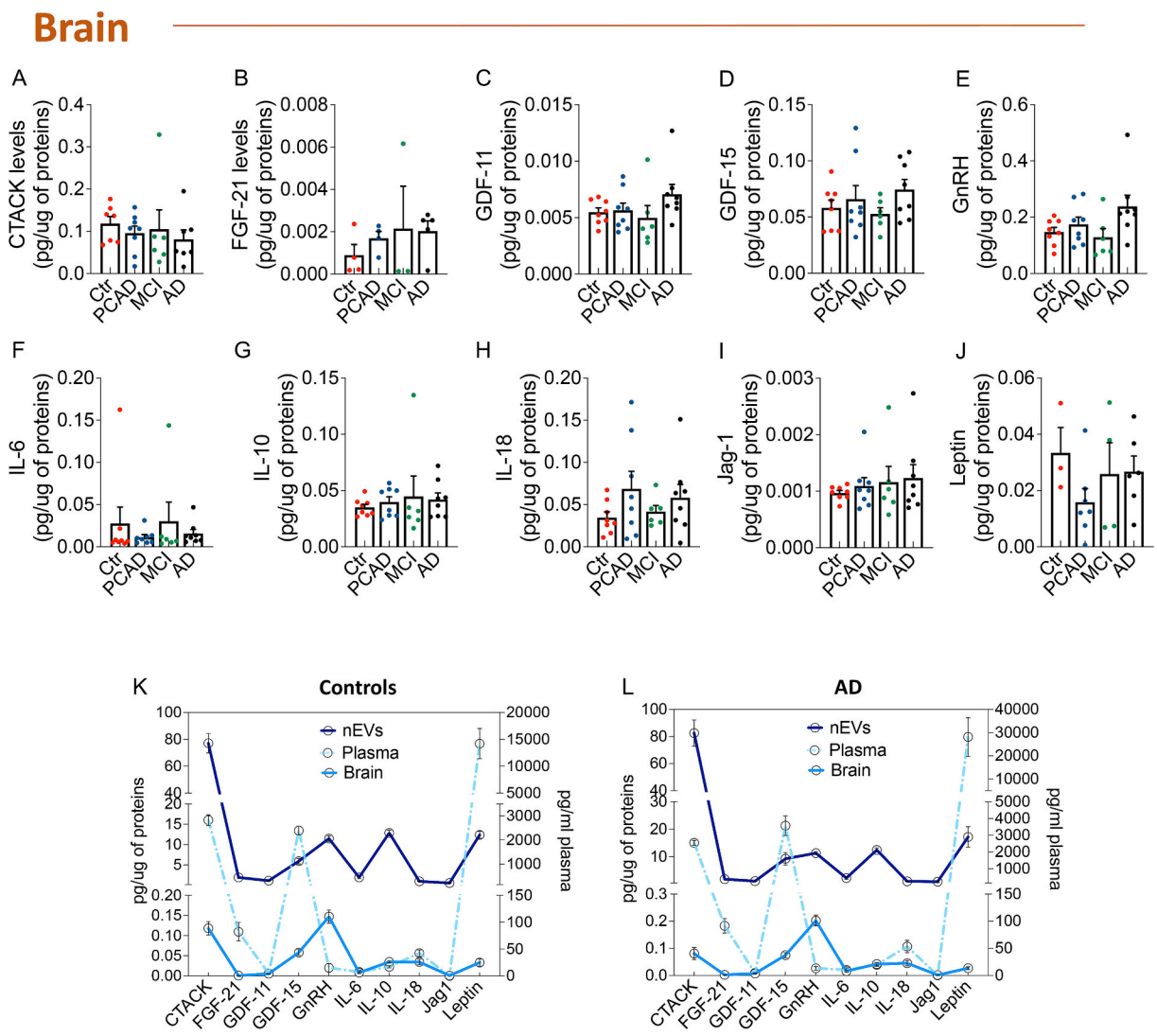


**Fig. 3.** Biomarker levels in post-mortem brain tissue across the AD continuum. (A–J) Levels of biomarkers measured in IPL brain tissue from control (CTR, $n = 8$), preclinical AD (PCAD, n = 8), mild cognitive impairment (MCI, $n = 6$), and AD subjects (n = 8). Data are presented as mean ± SEM. Group differences were tested using one-way ANOVA followed by Dunnet post-hoc test when normality assumptions were met; for non-normally distributed variables, the Kruskal–Wallis test was used followed by Dunn's corrections for multiple comparisons. In (K-L) mean values of biomarkers measured in nEVs, plasma, and post-mortem IPL brain samples from AD and Ctr subjects. The relative distribution across compartments indicates higher similarity between nEVs and brain profiles than between plasma and brain. Spearman correlations confirm this: in AD, ρ = 0.685 (nEVs–brain) and ρ = 0.430 (plasma–brain); in controls, ρ = 0.782 (nEVs–brain) and ρ = 0.491 (plasma–brain).

groups varied as a function of age. The interaction analysis yielded biomarker-specific results: a statistically significant age-by-diagnosis interaction was observed for GnRH (AGE×DIAGNOSI: β = 0.111 ± 0.020, z = 5.704, $p = 1.16e-8$, 95% CI 0.073–0.150), IL-6 (β = −0.079 ± 0.028, z = −2.790, $p = 0.005$, 95% CI −0.134 to −0.023), and Jag-1 (β = −0.041 ± 0.017, z = −2.375, $p = 0.017$, 95% CI −0.075 to −0.007) Supplementary Fig. 4A–C).

When applying the same age-by-diagnosis interaction model to plasma biomarkers, significant interactions were detected for FGF-21 (AGE×DIAGNOSI: β = 4.156 ± 0.290, z = 14.308, $p < 1.95e-4$; 95% CI 3.587–4.726), GDF-15 (β = 87.160 ± 19.306, z = 4.515, $p = 6.34e-6$; 95% CI 49.321–125.000), IL-10 (β = 1.285 ± 0.496, z = 2.591, $p = 0.00958$; 95% CI 0.313–2.257), and IL-18 (β = 3.736 ± 0.272, z = 13.752, $p = 4.98e-4$; 95% CI 3.204–4.269) (Supplementary Fig. 4D–G).

These results highlight that age significantly modulates the association between diagnosis and biomarker levels, both in nEVs and plasma. Age-related effects may obscure disease-related differences unless explicitly modeled using interaction approaches.

### 3.5. *nEVs biomarkers in Ctr subjects predict functional decline before AD onset*

Correlation analyses were conducted between biomarker levels measured in nEVs, plasma, or post-mortem brain samples and clinical scores to explore their association with functional and cognitive outcomes. In cognitively healthy Ctr subjects, several nEVs biomarkers were positively and significantly associated with one another (Fig. 4A). Furthermore, several biomarkers such as GDF-11, IL-6, IL-18, and Jag-1 showed significant and negative associations with ADL and IADL scores (Fig. 4A). These findings suggest that in the absence of overt neurodegeneration, the activation of shared biological pathways, including metabolic regulation, cellular stress response, and neuroimmune signaling (Jena et al., 2023; Liu et al., 2021; Wang et al., 2023; Nakamichi et al., 2025; Kapoor and Nation, 2021; Charisis et al., 2024), may reflect compensatory mechanisms aimed at preserving neuronal homeostasis and functional autonomy during the aging process. Notably, these associations were markedly weakened in the AD group, where the progression of neuropathological changes likely disrupts homeostatic

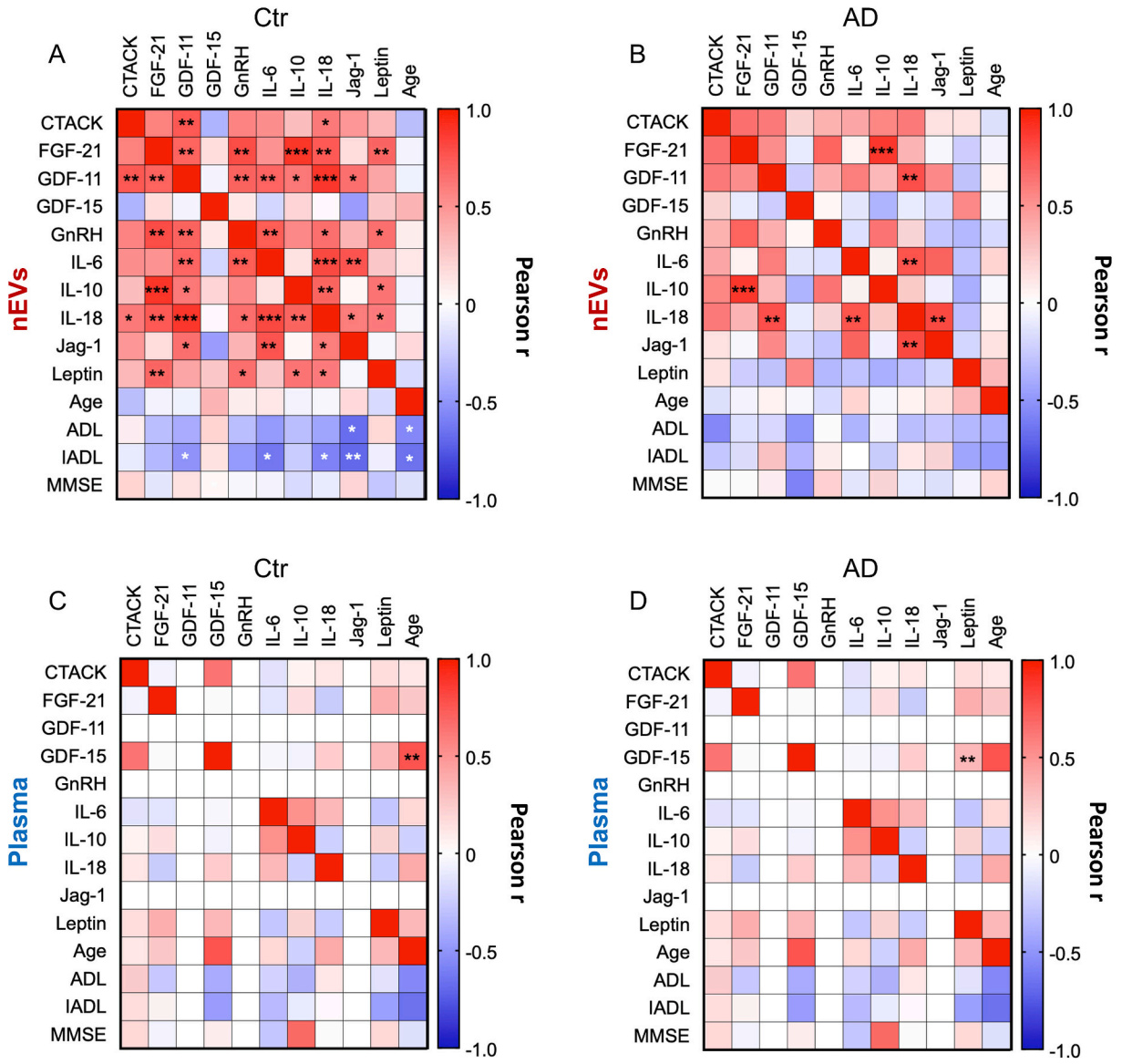


**Fig. 4.** Correlation analysis of biomarkers in nEVs and plasma from Ctr and AD subjects. (A–B) Pearson correlation matrices among nEV biomarkers in Ctr and AD groups. (C—D) Equivalent matrices for plasma biomarkers. Blue–white–red color scale represents Pearson's *r*. Asterisks indicate correlations that remain significant after Benjamini–Hochberg false discovery rate (FDR) correction: *, $p < 0.05$; **, $p < 0.01$; ***, $p < 0.001$. (For interpretation of the references to color in this figure legend, the reader is referred to the web version of this article.)

regulatory networks and diminishes the predictive power of these molecular signatures (Fig. 4B). By contrast, very few significant associations emerged from plasma measurements, including GDF-15 and age in Ctr subjects (Figs. 4C) and GDF-15 and Leptin in AD subjects (Figs. 4D).

This pattern supports the idea that nEVs provide insights into earlier molecular changes associated with functional decline, that are lost if the same markers are measured in plasma samples, likely due to the fact that plasma biomarkers are diluted by contributions from multiple tissues.

### *3.6. Correlations analyses in post-mortem IPL tissues support nEVs-derived findings*

To further strengthen the associations observed among nEVs-derived biomarkers and clinical outcomes, we replicated the same correlation analyses in post-mortem IPL tissue across different stages of the AD continuum. The rationale was to assess whether molecular patterns identified in circulating nEVs were also reflected at the tissue level, thereby reinforcing their biological relevance and translational potential as brain-derived proxies of neurodegeneration. Correlation patterns in IPL samples revealed a dynamic shift across disease stages (Fig. 5). Because of the limited number of brain samples, only a few correlations remained significant after FDR correction. Nevertheless, these correlations consistently converged on the same metabolic–neuroendocrine axis highlighted in nEVs. A strong positive association between GDF-11 and GnRH was evident in cognitively healthy individuals (Fig. 5A) and in PCAD (Fig. 5B), mirroring the coupling between these two markers observed in nEV-derived vesicles. This shared GDF-11–GnRH axis suggests that nEVs capture at least part of the coordinated signaling pattern present in the aging but non-demented brain. As the pathology progresses (MCI and AD) these associations shift toward inflammatory mediators including IL-6, IL-10, and Jag-1 (Figure C—D), indicating a breakdown of cellular homeostasis and the emergence of chronic neuroinflammation. This molecular reorganization peaked in the MCI group, where multiple biomarkers (CTACK, FGF-21, IL-6, IL-10, and Jag-1) were also significantly associated with MMSE scores (Fig. 5C). Overall, these post-mortem brain data are consistent with a progressive

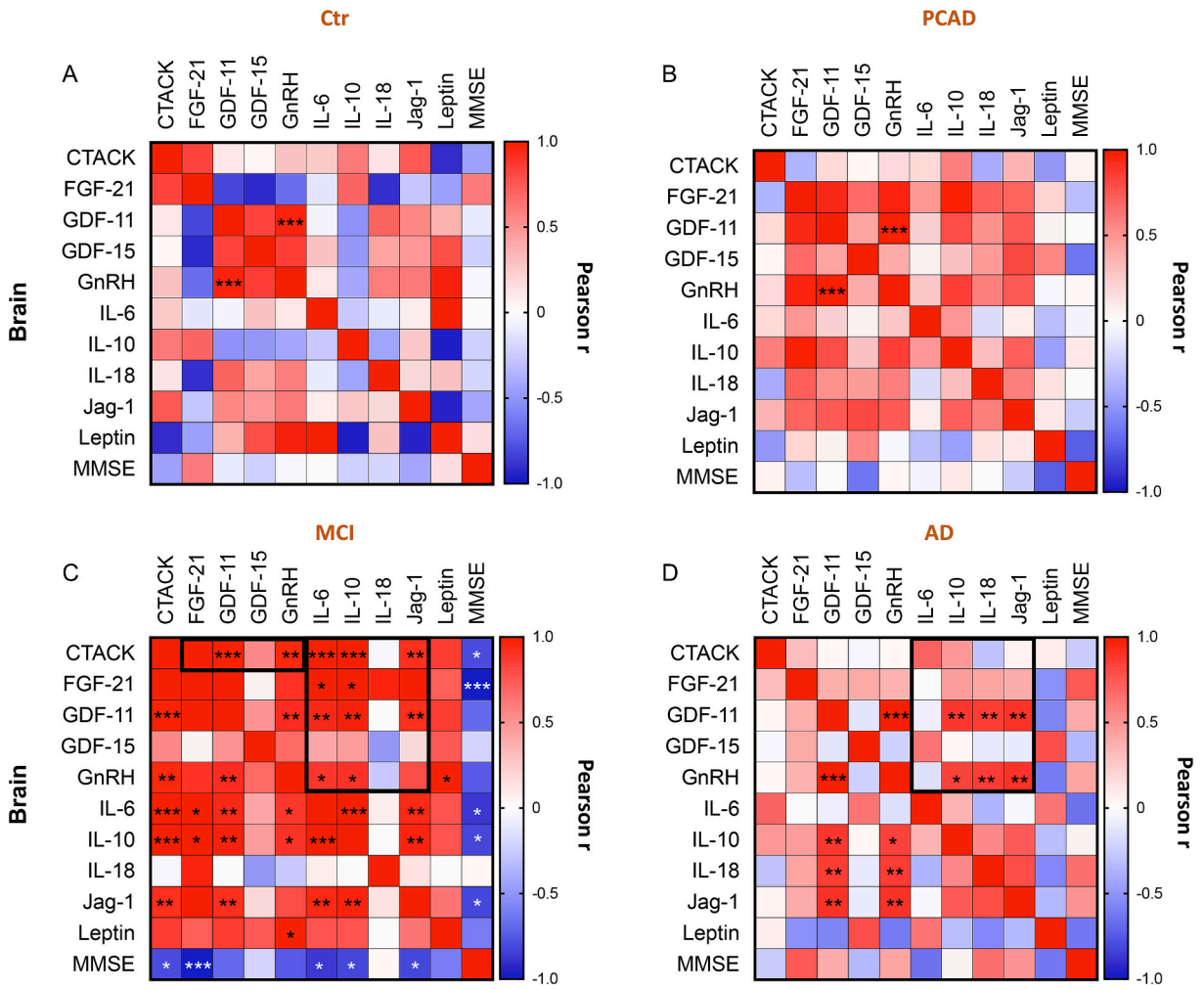


**Fig. 5.** Correlation analysis of biomarkers in post-mortem brain samples across the AD continuum. (A–D) Pearson correlation matrices for IPL brain biomarkers in Ctr, PCAD, MCI, and AD subjects. Blue–white–red color scale indicates Pearson's *r*. Asterisks indicate correlations that remain significant after Benjamini–Hochberg false discovery rate (FDR) correction: *, $p < 0.05$; **, $p < 0.01$; ***, $p < 0.001$. (For interpretation of the references to color in this figure legend, the reader is referred to the web version of this article.)

disruption of the coordinated biomarker relationships observed in aged cognitively normal individuals across the AD continuum. This transition is captured by nEVs, but not by plasma, and supports the ability of nEV-derived biomarkers to mirror brain-specific molecular changes and to track the shift from early, relatively regulated processes to the dysregulated state characteristic of AD pathology.

### *3.7. nEVs biomarkers reveal sex-associated differences in predicting cognitive decline*

Given the growing body of evidence suggesting that sex plays a critical role in the development and progression of AD (Oveisgharan et al., 2018; Rajan et al., 2021), we investigated potential sex-related differences in the levels of brain aging biomarkers measured in nEVs (Fig. 6A-J) and plasma (Fig. 6K-T). The analysis of nEVs showed a significant increase in GDF-15 levels in females with AD compared to males and a nearly significant increase compared to females in the CTR group (Fig. 6D). Rather, males with AD were characterized by significantly elevated levels of IL-6, IL-18, and Jag-1 (Fig. 6F, H, and I). Measures performed in plasma samples showed a significant increase in GDF-15 levels in females with AD (Fig. 6N), while a significant increase in IL-10 was observed in males with AD (Fig. 6Q). Regression analyses (Supplementary Fig. 5) showed that only GDF-15 and Leptin plasma levels predicted nEVs levels in both males and females (Supplementary Figs. 5C and 5G), confirming the results observed in the whole cohort. Intriguingly, increased GDF-15 levels in nEVs were associated with worse functional outcome measures in females (Figs. 7B), suggesting a greater relevance of mitochondrial stress-related AD pathology among women.

Taken together, these findings indicate that nEV-derived biomarkers capture sex-specific vulnerability patterns, with GDF-15–related mitochondrial stress emerging as a stronger determinant of functional and cognitive decline in women, and IL-6/IL-18/Jag-1–linked immune–metabolic dysregulation playing a more prominent role in men.

### *3.8. Identification of a minimal nEVs-derived biomarkers panel to discriminate AD from Ctr subjects*

Building on our previous analyses of biomarker variations in relation to aging, AD pathology, and sex differences, we next sought to integrate these factors into a unified model. Specifically, we aimed to identify a minimal panel of nEV-derived biomarkers capable of distinguishing AD from Ctr subjects, while accounting for key demographic variables (age and sex) and clinical measures (ADL, IADL, and MMSE). This integrative approach was designed to enhance the diagnostic utility of the biomarkers by capturing their combined predictive value in a multidimensional framework. A preliminary Lasso Logistic Regression-based analysis revealed that GDF-11, GDF-15, Jag-1, Leptin, age, and sex were

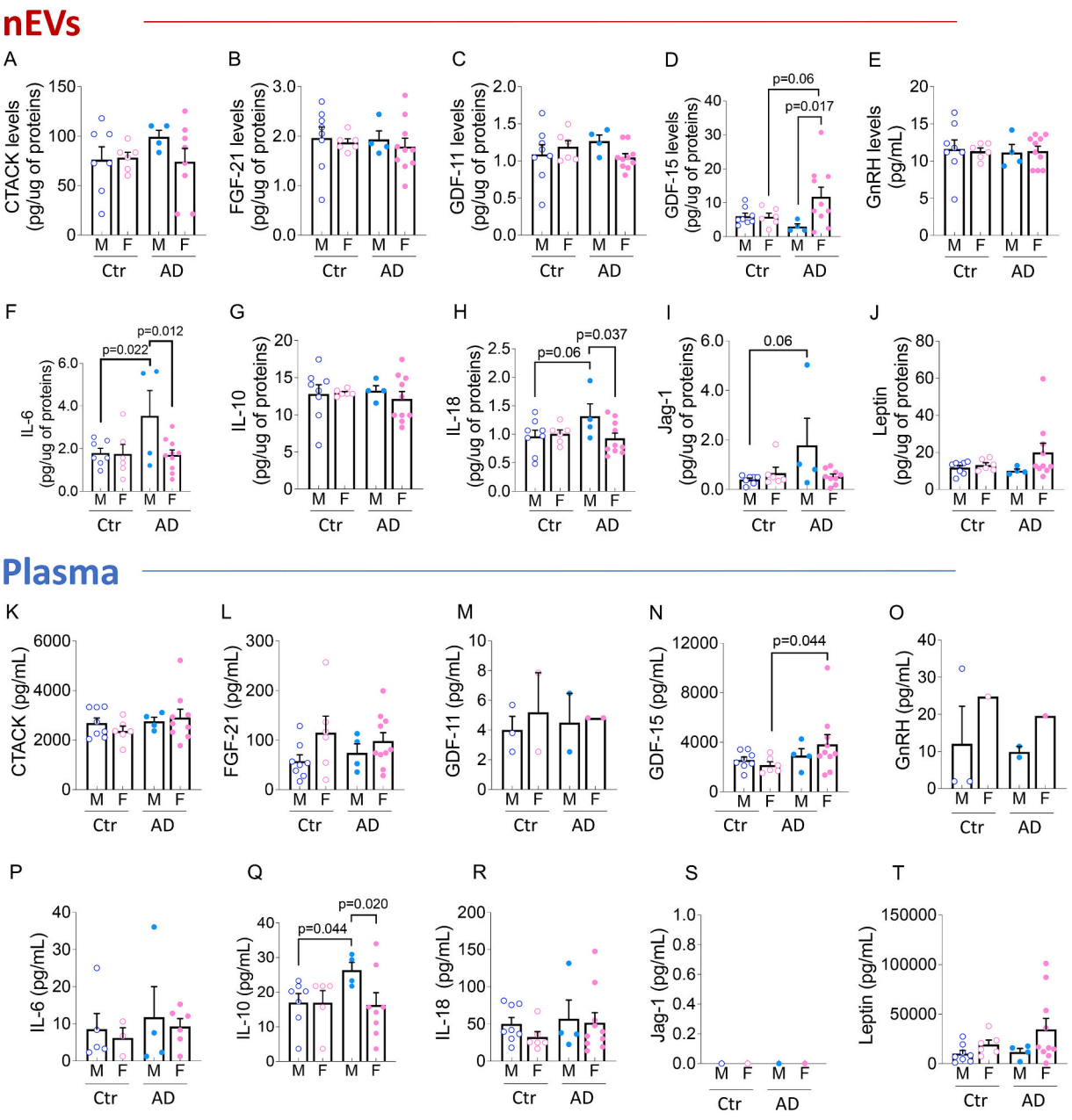


**Fig. 6.** Sex-specific differences in biomarker levels in nEVs and plasma. (A–J) Comparison of biomarker levels in nEVs isolated from Ctr (males, n = 8 and females, n = 6) and AD (males, $n = 4$ and females, n = 10) subjects. (K–T) Same comparison in plasma samples. Data shown as mean ± SEM. Group differences across sex/diagnosis were tested using one-way ANOVA when normality assumptions were met, followed by a priori planned comparisons using Fisher's LSD; for non-normally distributed variables, the Kruskal–Wallis test was used, followed by Dunn's planned comparisons (no multiplicity adjustment). For panels with annotated *p*-values, omnibus test statistics and planned-comparison p-values are reported below: GDF-15 (nEVs): one-way ANOVA F (Triani et al., 2018; Muehlboeck et al., 2014)=2.91, $p = 0.0550$; Fisher's LSD: AD females vs AD males $p = 0.017$, AD females vs Ctr females $p = 0.060$. IL-6 (nEVs): one-way ANOVA F (Triani et al., 2018; Jack Jr. et al., 2024)=2.83, $p = 0.0609$; Fisher's LSD: AD males vs Ctr males $p = 0.022$, AD males vs AD females $p = 0.012$. IL-18 (nEVs): one-way ANOVA F (Triani et al., 2018; Muehlboeck et al., 2014)=1.74, $p = 0.1863$; Fisher's LSD: AD males vs Ctr males p = 0.060, AD males vs AD females $p = 0.037$. Jag-1 (nEVs): Kruskal–Wallis H = 3.391, $p = 0.3351$; Dunn's planned comparisons: Ctr males vs AD males p = 0.060. GDF-15 (plasma): Kruskal–Wallis H = 4.420, $p = 0.2196$; Dunn's planned comparisons: Ctr females vs AD females $p = 0.044$. IL-10 (plasma): Kruskal–Wallis H = 5.86, $p = 0.1185$; Dunn's planned comparisons: Ctr males vs AD males $p = 0.046$, AD males vs AD females $p = 0.020$.

the most informative predictors for distinguishing AD from Ctr subjects. Notably, after adjusting for age and sex, GDF-15, Jag-1, and Leptin levels were all found to be higher while GDF-11 levels were lower in AD subjects compared to Ctr. These directional effects reflect the coefficients estimated by the regularized logistic regression model. To assess whether the selected molecules naturally grouped Ctr and AD subjects into distinct clusters, we applied K-means clustering. This analysis showed a Silhouette score of 0.68, indicating a well-defined cluster structure and suggesting that the selected biomarkers effectively capture the underlying differences between Ctr and AD subjects. Furthermore, performing a logistic regression classification using age-residualized biomarkers achieved 67% accuracy, with a precision of 0.75 for AD and 0.60 for Ctr. The model correctly identified 60% of AD cases and 75% of Ctr participants, confirming its predictive ability, but also indicating room for improvement. The most significant predictors were GDF-15 (importance: 0.18), sex (0.12), Leptin (0.10), and Jag-1

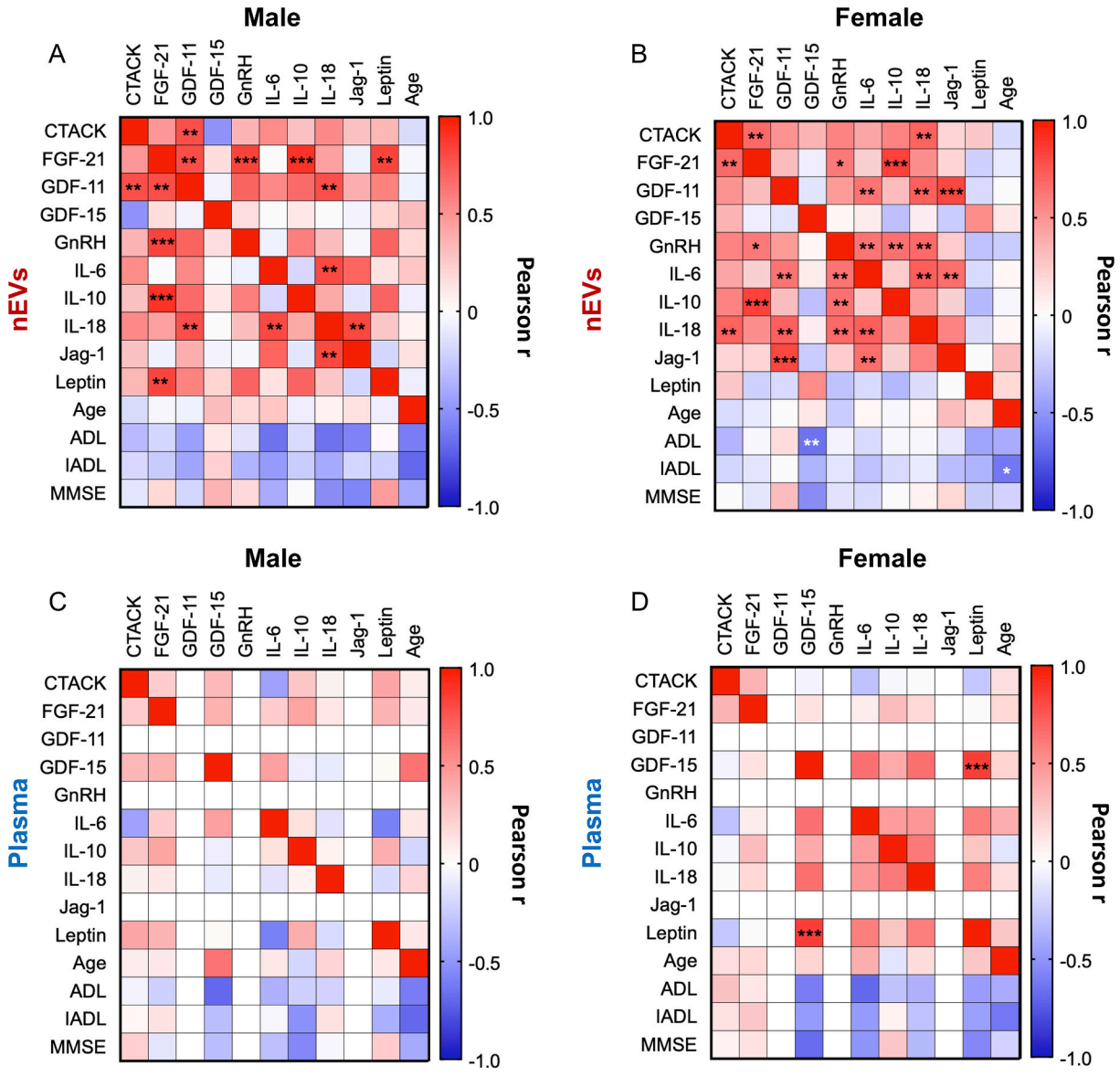


**Fig. 7.** Sex-stratified correlation matrices for nEVs and plasma biomarkers. (A–B) Pearson correlation matrices among nEV biomarkers in males and females subjects. (C—D) Equivalent analysis in plasma. Blue–white–red color scale represents Pearson's *r*. Asterisks indicate correlations that remain significant after Benjamini–Hochberg false discovery rate (FDR) correction: *, $p < 0.05$; **, $p < 0.01$; ***, $p < 0.001$. (For interpretation of the references to color in this figure legend, the reader is referred to the web version of this article.)

(0.09), reinforcing the role of these biomarkers in distinguishing Ctr from AD. Interestingly, the minimal panel of biomarkers includes candidates, that were previously found to be independently associated with aging (Jag-1, Supplementary Fig. 4), cognitive performance (GDF-11 and Jag-1, Fig. 4), and sex (GDF-15 and Jag-1, Fig. 6) in nEVs. To ensure the robustness of the model, we also evaluated the degree of multicollinearity among predictors. Variance Inflation Factor (VIF) analysis indicated acceptable levels of collinearity, i.e. < 5, across most variables in the nEV-based model, supporting the reliability of the selected features. This step confirmed that the predictive capacity of the panel was not driven by redundancy among biomarkers, but by complementary biological information.

This analysis identified a minimal panel of four age- and sex-adjusted nEV-derived biomarkers (lower GDF-11, and higher GDF-15, Jag-1, and Leptin levels) that allows the discrimination between AD and control participants, supporting their combined use as a biologically coherent signature rather than as isolated predictors.

### *3.9. The nEV-derived biomarker panel shows limited discriminative performance in plasma*

We conducted the same analysis using biomarker data derived from plasma samples. After identical preprocessing steps, Lasso Logistic Regression selected GDF-15, CTACK, IL-10, age, and sex as the most relevant features for classifying AD and Ctr subjects. K-means clustering based on these plasma biomarkers yielded a Silhouette score of 0.53, indicating a moderate clustering structure. The logistic regression model built on age-residualized plasma biomarkers achieved an overall classification accuracy of 11.1%, with a precision below 0.20 for AD and Ctr. These results indicate limited classification performance, possibly due to the small sample size or high biomarker variability in plasma. Finally, the VIF values for the biomarkers and variables were within an acceptable range (<5), indicating that multicollinearity is unlikely to significantly affect the model's reliability.

Overall, these results indicate that the same biomarker panel, when measured in plasma, shows poor discriminative performance between

AD and control subjects, underscoring the added value of nEVs enrichment for capturing brain-related molecular signatures.

### 3.10. Post-mortem brain biomarkers show limited clustering but converge with nEVs on key predictors

To unravel whether the identified significant predictors in nEVs (GDF-11, GDF-15, Jag-1, Leptin, age, and sex) are consistent in post-mortem brain samples, similar analyses were performed between Ctr and MCI – being the group characterized by the stronger associations among some biomarkers and cognitive performance – and between Ctr and AD, which are the same diagnostic groups from which nEVs were isolated. Lasso Logistic Regression identified Jag-1, GDF-11, IL-18 and age as the most predictive features distinguishing Ctr from MCI. These variables were subsequently employed in a K-means clustering analysis, which resulted in a maximum Silhouette score of 0.44, indicating a poor clustering structure and limited discriminative power between Ctr and MCI groups. Similarly, Lasso Logistic Regression identified GnRH, CTACK, FGF-21, GDF-15, and age as the most predictive features for distinguishing Ctr from AD subjects. K-means clustering analysis yielded a maximum Silhouette score of 0.38. This score indicates a poor clustering structure, suggesting that the clustering did not effectively differentiate between the AD and Ctr groups. VIF analysis in both models revealed considerable multicollinearity among several predictors, suggesting that linear dependencies may limit the distinct contribution of individual biomarkers in these tissue-based analyses.

While analyses on post-mortem brain samples did not achieve the same level of clustering resolution, they nonetheless revealed the presence of meaningful predictors distinguishing Ctr from both MCI and AD groups. Importantly, several biomarkers identified as relevant in nEVs, such as GDF-11, GDF-15 and Jag-1, as well as age, also emerged as significant predictors in post-mortem brain analyses. This convergence across independent biospecimens reinforces the biological significance of these biomarkers and supports their potential translational value in tracking neurodegenerative changes. Moreover, these findings underscore the potential of nEV-derived biomarkers in the development of precision diagnostics for early-stage neurodegeneration, while highlighting the complementary role of brain tissue studies in validating and contextualizing biomarker-based discoveries in broader and more diverse cohorts.

### 3.11. Aging biomarkers in plasma and nEVs correlate with brain structural alterations in a subgroup of cognitively normal subjects

The biological significance of aging-associated biomarkers was investigated through correlation analyses between their levels (measured in nEVs or plasma) and MRI-derived brain structural parameters in a subgroup of cognitively normal participants ($n = 7$) for whom MRI data were available. Despite the limited sample size of cognitively normal subjects with available MRI data, the correlation analysis revealed robust and biologically consistent associations between aging-related biomarkers measured in nEVs and structural brain alterations typically observed in aging and AD. To systematically explore these associations, we generated hierarchical cluster heatmaps of the significant Pearson correlations ($p < 0.05$), grouping brain regions and biomarkers based on similarity in their correlation profiles. This unsupervised approach highlighted distinct clusters of brain regions that showed convergent relationships with specific biomarkers, particularly in the temporo-limbic and associative cortical areas known to be early targets of AD-related neurodegeneration (Wen et al., 2025a; Keith et al., 2024). To provide a spatial representation of these associations, we generated anatomical brain maps displaying significant correlations between nEVs or plasma biomarkers and MRI-derived structural measures. These results are shown in Fig. 8 (for nEVs) and Supplementary Fig. 6 (for plasma). nEV biomarkers consistently highlight the regional specificity and directionality of the associations, particularly in temporo-limbic and associative cortical areas typically affected in aging and AD. Full results are reported in Supplementary Table 3 and visualized in Supplementary Figs. 7–10. Notably, all four biomarkers that comprise the minimal predictive panel—GDF-11, GDF-15, Jag-1, and Leptin—exhibited consistent and biologically meaningful associations with structural brain alterations. These included widespread negative correlations with cortical thickness and volume in regions such as the entorhinal cortex, middle and inferior temporal gyri, fusiform and parahippocampal regions, and hippocampal subfields (e.g., rh_fusiform_volume: $r = -0.9446$, $p < 0.01$; lh_entorhinal_thickness: $r = -0.834$, $p < 0.05$; right_CA3: $r = -0.779$, $p < 0.05$). These regions are classically involved in the early stages of AD-related neurodegeneration. Beyond temporo-limbic atrophy, these biomarkers were also associated with alterations in associative and paralimbic cortices, including the frontal pole, insula, and superior parietal lobule, suggesting diffuse vulnerability and involvement in broader networks of age-related structural decline. A subset of associations also pointed to positive correlations with occipital surface area (e.g., lh_pericalcarine_area: $r = 0.9136$, $p < 0.01$ for GDF-11), potentially reflecting compensatory cortical reorganization. Importantly, several of these biomarkers, especially Jag, also correlated with visual rating scores derived from T1-weighted MRI (e.g., mta_right_model_4: $r = 0.9097$, $p < 0.01$), reinforcing their relevance to clinically interpretable indices of medial temporal atrophy. These associations were consistently stronger and more anatomically specific in nEVs than in plasma, underscoring the superior sensitivity and brain-representativeness of nEVs-derived biomarkers. The observed clustering of biologically meaningful associations supports the utility of nEVs not only as carriers of aging signals but also as precise molecular mirrors of brain structure. While these results are clearly exploratory due to the very small sample size and the absence of sex-stratified analyses, they provide preliminary evidence that peripheral molecular signatures, particularly those extracted from nEVs, may reflect in vivo neuroanatomical variation and could serve as early indicators of neurodegenerative risk, pending confirmation in larger cohorts.

## 4. Discussion

Our findings demonstrate that nEVs represent a powerful and biologically specific source of peripheral biomarkers to track brain aging and AD progression. Across all analytical domains, including age, sex, cognitive function, and MRI, nEV-derived biomarkers consistently outperformed plasma-derived measures, confirming their closer link to central nervous system processes.

We successfully isolated and validated nEVs using an established protocol, confirming their neuronal origin through size profiling, EV biomarker enrichment, and L1CAM specificity (Manolopoulos et al., 2025; Perluigi et al., 2022; Kapogiannis et al., 2024; Nogueras-Ortiz et al., 2024). A critical challenge in biomarkers research is the confounding effect of chronological age (Moqri et al., 2023). Importantly, age-by-diagnosis interaction models revealed disease-specific deviations from normal aging trajectories (GnRH, IL-6, and Jag-1 in nEVs; and FGF-21, IL-10, and GDF-15 in plasma), suggesting that disease effects may be obscured unless age is explicitly modeled. This observation reinforces the idea that certain molecular signatures in AD reflect a “accelerated aging” rather than chronological aging alone. Notably, the effects of age and diagnosis were more distinctly resolved in nEVs than in plasma, underscoring the specificity of nEVs for tracking brain-derived alterations.

One of the strengths of our work was to compare the levels of the evaluated biomarkers between nEVs and plasma samples from the same subjects. Compared to plasma, nEVs revealed a superior power in distinguishing Ctr vs AD subjects. nEV-derived biomarkers exhibited a coordinated expression pattern and few of them, GDF-11, IL-6, IL-18, and Jag-1, were independently associated with reduced autonomy and daily functioning, even before overt cognitive decline becomes

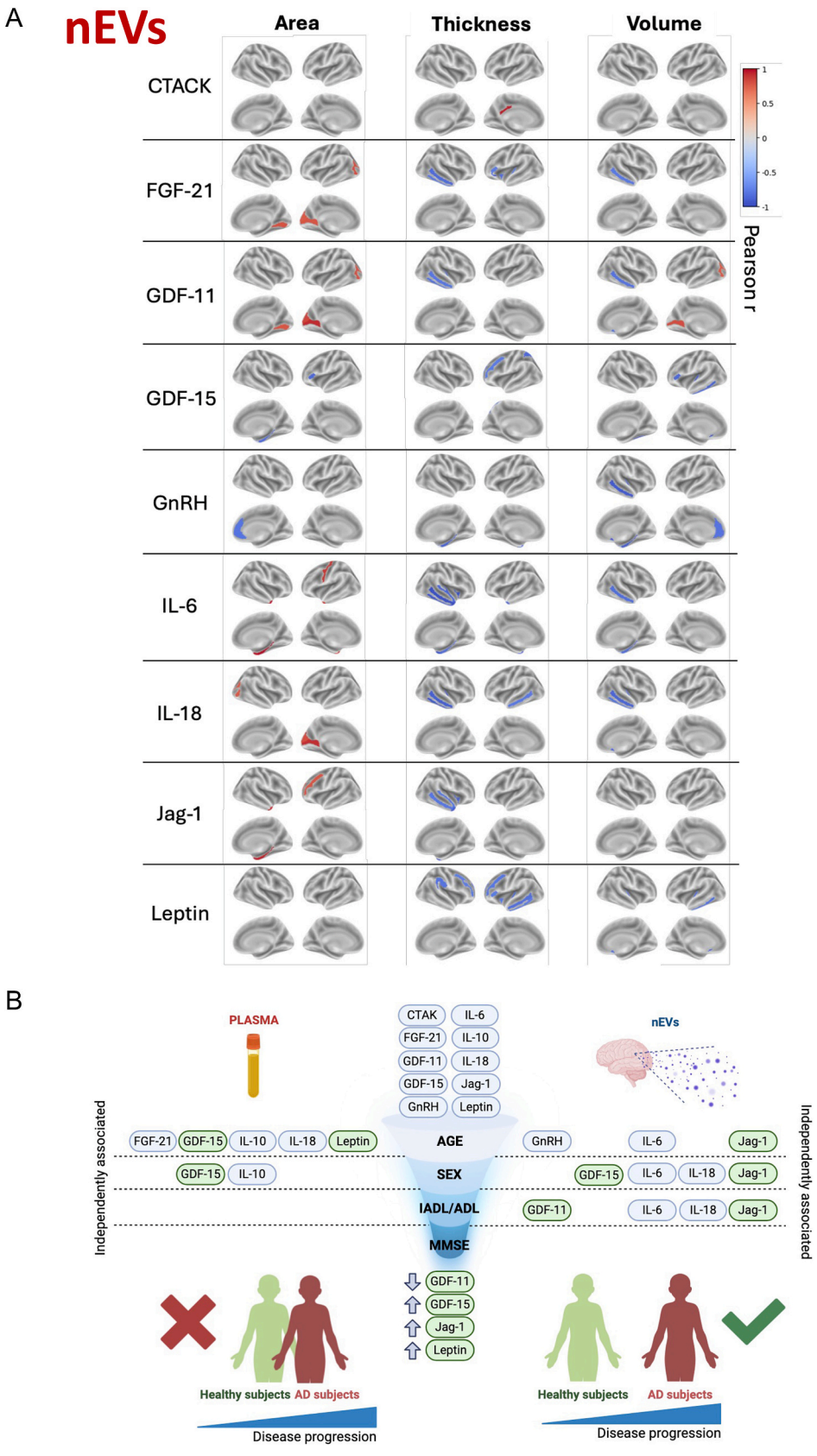


(caption on next page)

**Fig. 8.** Brain maps showing significant Pearson correlations between nEVs biomarker levels and MRI-derived structural measures, including cortical thickness, surface area, and regional volumes. (A) Regions are color-coded based on the direction and strength of the correlation (red: positive; blue: negative), and are displayed on lateral and medial views of both hemispheres. Only regions showing statistically significant associations ($p < 0.05$) are visualized. Anatomical labeling is based on the Desikan-Killiany atlas (FreeSurfer v6.0). Biomarkers included in this figure were selected based on their significant associations with MRI measures as reported in Supplementary Table 3. In (B) Scheme of biomarker associations across compartments, clinical variables, and disease stages. Measured biomarkers were independently associated with age, sex, functional (ADL/IADL), and cognitive (MMSE) outcomes, measured in plasma (left) and nEVs (right). Biomarkers included in the minimal predictive panel (GDF-11, GDF-15, Jag-1, and Leptin) are highlighted in green. The funnel shape represents the integration of demographic and clinical variables into the modeling pipeline. The bottom panels illustrate the stratification performance of plasma versus nEVs, where only nEV-derived markers reliably differentiate healthy individuals from AD subjects, as indicated by the green checkmark. The figure highlights the greater biological coherence, clinical relevance, and disease stratification capacity of nEV-derived biomarkers compared to plasma. (For interpretation of the references to color in this figure legend, the reader is referred to the web version of this article.)

detectable through standard cognitive screening tools such as the MMSE. Conversely, the observation that plasma levels of some biomarkers, i.e., CTACK, GDF-15, IL-6, and Leptin, correlate with MMSE but not with functional scales suggests that plasma biomarkers may reflect later-stage, systemic manifestations of the disease. These results support a temporal stratification of biomarker utility (Kapogiannis et al., 2019; Manolopoulos et al., 2023; Moqri et al., 2023): nEVs capture early, brain-specific dysfunction preceding cognitive impairment, while plasma biomarkers reflect later, more systemic manifestations of AD.

This pattern was mirrored in IPL post-mortem brain samples (Wen et al., 2025a; Keith et al., 2024), where similar shifts from metabolic to inflammatory profiles were observed along the AD continuum. Cognitively normal individuals exhibited significant correlations primarily among biomarkers involved in metabolism and cell growth, such as GDF-11, GDF-15, and Leptin, suggesting coordinated homeostatic regulation. However, as the disease progressed to MCI and AD, these associations weakened or were replaced by significant correlations with inflammatory cytokines, including IL-6, IL-10, and Jag-1. This transition reflects the increasing disruption of metabolic and cellular homeostasis and the emergence of chronic inflammation as a dominant feature of neurodegeneration (Butterfield and Halliwell, 2019). Importantly, this evolving molecular architecture was mirrored in nEVs but not in plasma, further underscoring the brain-like fidelity of nEV-derived profiles. While plasma correlations remained sparse and inconsistent across disease stages, nEVs recapitulated the brain's molecular trajectory, confirming their relevance for capturing dynamic, disease-related biological processes.

Sex-stratified analyses uncovered distinct biomarker trajectories associated with AD progression (Oveisgharan et al., 2018; Castro-Aldrete et al., 2025; Huque et al., 2023). In women, elevated GDF-15 levels in both plasma and nEVs were linked to worse cognitive and functional outcomes, pointing toward a prominent role of metabolic dysregulation in women with AD pathology (Liu et al., 2025; Demetrius et al., 2021). Conversely, in men, inflammatory biomarkers such as IL-6, IL-18, and Jag-1 were significantly elevated and associated with cognitive decline (Liu et al., 2025; Demetrius et al., 2021). These findings corroborate existing literature on sex-differential vulnerability in AD and emphasize the need for sex-specific biomarker frameworks to inform tailored diagnostic and therapeutic strategies. Remarkably, sex and APOE genotype have been reported to influence EV abundance, and in some settings also EV cargo profiles (Peng et al., 2019; Huang et al., 2025; Noren Hooten et al., 2022; Kim et al., 2022), raising the possibility of confounding when interpreting sex-stratified biomarker patterns. APOE genotype was not available in this cohort, and the sample size limits robust genotype- or sex-by-genotype stratification. Notably, our biomarker measurements were normalized to standardized protein input and thus primarily capture cargo composition rather than EV yield; while this approach does not fully exclude yield-related confounding, it is consistent with the interpretation that the observed differences reflect cargo-level alterations and warrants confirmation in larger, genotyped cohorts.

To integrate all the aspects emerged in our study, we identified a minimal predictive panel comprising four nEV-derived biomarkers – GDF-11, GDF-15, Jag-1, and Leptin – along with age and sex, that effectively distinguished Ctr from AD subjects. Each component of the panel had been previously linked to age-related change, cognitive function, or sex-specific effects in our dataset, suggesting that their selection was biologically meaningful rather than merely statistical. The model outperformed the plasma-based model which exhibited poor classification power. The relevance of this set of biomarkers is significant for several reasons. GDF-11 has been associated with neurogenic and vasculoprotective effects; its decline in aging correlates with reduced neurogenesis and impaired vascular remodeling, both of which contribute to cognitive deterioration (Katsimpardi et al., 2014). Elevated GDF-15 levels have been associated with poor cognitive outcomes and frailty in elderly individuals, particularly women (Liu et al., 2025; Conte et al., 2022; Chiariello et al., 2022). Alterations in Notch-Jag-1 signaling impair neurogenesis and contribute to synaptic loss and cognitive decline (Ables et al., 2011; Lampada and Taylor, 2023). In parallel, altered leptin levels have been associated with increased risk of dementia and hippocampal atrophy (Charisis et al., 2024; Lieb et al., 2009). Intriguingly, a U-shaped relationship was observed between circulating leptin levels and cognitive function, whereby both low and high leptin concentrations in older adults are associated with an increased risk of cognitive impairment (Annweiler et al., 2019). The combined predictive value of these biomarkers likely reflects the interplay between metabolic resilience, neurovascular integrity, inflammation, and neuroplasticity—domains whose disruption synergistically accelerates brain aging and predisposes to AD (Perluigi et al., 2024; Moqri et al., 2023). Beyond their individual associations with metabolic resilience, neuroinflammation, and vascular homeostasis, several components of the minimal predictive panel show mechanistic links to core AD pathologies. GDF-11 has been implicated in preserving synaptic integrity and reducing Aβ deposition in preclinical models, partly through enhanced neurogenesis and improved cerebrovascular function (Jiang et al., 2025). Conversely, elevated GDF-15 has been associated with mitochondrial stress and inflammatory signaling, pathways known to exacerbate tau phosphorylation and accelerate neurodegenerative cascades (Wen et al., 2025b). Jag-1, a key ligand in the Notch signaling pathway, influences neuronal differentiation and synaptic maintenance; dysregulation of Notch-Jag-1 signaling has been shown to promote both Aβ accumulation and tau-related synaptic dysfunction (Kapoor and Nation, 2021). Altered leptin signaling has similarly been linked to impaired Aβ clearance and heightened vulnerability of hippocampal circuits, providing a plausible explanation for its strong association with medial temporal atrophy in our cohort (Ormazabal et al., 2025). These converging biological roles suggest that the identified panel captures upstream processes that interact with and potentially modulate amyloid and tau pathology. From a translational viewpoint, combining this nEV-derived panel with established AD biomarkers such as Aβ42/40, p-tau181 or p-tau217, and NfL may enhance diagnostic accuracy, particularly in the preclinical and prodromal stages where metabolic and inflammatory alterations precede overt neuronal loss. Such multimodal integration could refine risk stratification, improve the temporal resolution of disease staging, and ultimately support precision-medicine algorithms for early detection and intervention.

Correlations between nEV-derived biomarker levels and MRI-based cortical metrics in cognitively normal individuals provide additional

support for the neurobiological relevance of the identified minimal predictive panel. Specifically, the four selected biomarkers, GDF-11, GDF-15, Jag-1, and Leptin, exhibited consistent and anatomically specific associations with structural brain changes in regions classically involved in early AD, including reduced hippocampal volume and decreased cortical thickness in the temporal pole, insula, and medial temporal lobe (Wen et al., 2025a; Keith et al., 2024). GDF-15 and Leptin, both related to metabolic regulation, mapped onto.

medial temporal thinning and hippocampal atrophy, aligning with their proposed role in energy imbalance and neurodegeneration (Charisis et al., 2024; Liu et al., 2025; Conte et al., 2022; Chiariello et al., 2022; Lieb et al., 2009; Annweiler et al., 2019; Maioli et al., 2015; Mancuso et al., 2011). Jag-1 showed specific associations with reduced thickness in the cingulate and lateral temporal areas, consistent with its involvement in neuroinflammatory and Notch signaling pathways (Ables et al., 2011; Lampada and Taylor, 2023). GDF-11 was primarily associated with structural alterations in parietal and occipital cortices, suggesting a broader pattern of network-level vulnerability (Katsimpardi et al., 2014). Notably, these associations emerged more robustly and with clearer anatomical specificity when these biomarkers were measured in nEVs rather than plasma, further highlighting the brain-derived nature of these vesicular signals.

Together, these findings reinforce the notion that nEV-based biomarkers are capable of non-invasively capturing spatially resolved structural brain changes, and that the components of the minimal panel map onto known AD-related neuroanatomical trajectories even before clinical symptoms emerge.

## 5. Limitations and methodological considerations

The current study has some limitations. Given the small sample size, the statistical power to detect an Age × Group interaction is limited. However, this was a pilot study, and as such, the sample size was intentionally kept limited to assess feasibility, generate preliminary insights, and identify promising biomarker candidates for future validation. Expanding the age range from the current 54–89 years to a broader span (e.g., 10–90 years) would increase the estimated power from approximately 0.09 to 0.24. However, this remains well below the conventional threshold of 0.80, indicating that both a larger sample size and a broader age distribution would be necessary to reliably detect meaningful interaction effects. Cross-sectional design constrains causal inferences, and potential confounding by comorbidities, medication, or vascular pathology cannot be excluded. Hence, future work should focus on validating these findings in larger, longitudinal cohorts with diverse demographic and clinical profiles. Integration with neuroimaging, CSF/plasma biomarkers currently used in clinics, and genetic data could enhance predictive models.

In addition, a methodological consideration concerns the normalization strategy used for nEV readouts. In this study, biomarker levels in immunocaptured nEVs were expressed per μg of total protein from the L1CAM-immunocapture eluate (Bradford), reflecting our primary objective to compare biomarker abundance per unit of captured neuronal EV–derived material across subjects under standardized conditions. This approach is conceptually aligned with common EVs immunoblotting and proteomics workflows, where comparisons are typically made using a controlled amount of input material. Importantly, MISEV guidelines (Welsh et al., 2024; Thery et al., 2018) recognize that EV abundance can be approximated using particle number, protein content and/or lipid content, and they do not prescribe a single universal “gold standard” denominator for all applications. Normalization to particle count can be informative when the research question specifically addresses EVs concentration or vesicle release; however, it also implicitly assumes that each counted particle carries comparable protein cargo—an assumption that may not hold in heterogeneous EVs preparations. In such settings, particle-number normalization may introduce bias if cargo loading varies across vesicles and conditions. In contrast, normalizing to a fixed amount of eluate-derived protein ensures that biomarker measurements are compared across equivalent amounts of captured material under controlled loading conditions. Accordingly, our conclusions are framed in terms of differences in biomarker abundance per unit of immunocaptured nEV-derived protein rather than differences in EV particle release. Future studies designed to directly address EVs yield and cargo-per-vesicle relationships will benefit from systematic particle quantification across the full cohort and orthogonal normalization strategies.

## 6. Conclusions

In conclusion, our results suggest that nEVs constitute a promising source to inform about brain aging and neurodegeneration. They not only reflect molecular patterns observed in the brain but also are associated with cognitive decline and track structural brain changes more strongly than plasma biomarkers in this cohort. Importantly, they highlight sex-associated patterns and enable classification of disease state with modest but promising accuracy using minimal biomarker panels. The translational value of these findings lies in the potential of nEVs to serve as liquid biopsies for the brain, capable of identifying early and sex-differentiated biomarkers of neurodegenerative risk. Future studies should validate these results in larger, independent cohorts and explore longitudinal applications of nEV profiling in clinical trials. The integration of neuroimaging, genetic, and cognitive data with nEV-based biomarkers may ultimately enhance our capacity to predict, monitor, and treat age-related neurodegenerative conditions with greater precision.

## CRediT authorship contribution statement

**Simona Lanzillotta:** Visualization, Methodology, Investigation, Formal analysis, Data curation. **Virginia Boccardi:** Writing – review & editing, Writing – original draft, Validation, Methodology, Investigation, Funding acquisition, Formal analysis, Data curation. **Barbara Zulli:** Methodology, Investigation. **Alessandro Napoli:** Software, Methodology, Investigation, Formal analysis. **Gabriele Paolozzi:** Visualization, Software, Methodology, Investigation. **Roberta Angelini:** Methodology, Investigation. **Barbara Ruzicka:** Methodology, Investigation. **Federica Fratini:** Methodology, Investigation. **Anna Giulia Guazzarini:** Methodology, Investigation. **Michela Scamosci:** Methodology, Investigation. **Patrizia Bastiani:** Methodology, Investigation. **Martina Alunno:** Methodology, Investigation. **Eric Westman:** Writing – review & editing, Validation. **Fabio Di Domenico:** Writing – review & editing, Methodology, Investigation. **Marzia Perluigi:** Writing – review & editing, Methodology, Investigation. **Antonella Tramutola:** Writing – review & editing, Methodology, Investigation. **Roberta Cecchetti:** Methodology, Investigation. **Tommaso Mazza:** Writing – review & editing, Software, Formal analysis, Data curation. **D. Allan Butterfield:** Writing – review & editing, Validation. **Patrizia Mecocci:** Writing – review & editing, Writing – original draft, Supervision, Project administration, Funding acquisition, Formal analysis, Data curation, Conceptualization. **Eugenio Barone:** Writing – review & editing, Writing – original draft, Visualization, Supervision, Software, Project administration, Funding acquisition, Formal analysis, Data curation, Conceptualization.

## Ethics approval

Participants recruited provided informed consent, and the study adhered to the Declaration of Helsinki and was approved by the Regional Ethical Committee (Prot. N. CE-1065/24 del 24/07/2024). Consent for inclusion in the study was obtained during a visit to outpatient clinics from all participants and was archived for participation/publication.

## Fundings

This work has been supported by Fondi Ateneo grants funded by Sapienza University (#SP1221844C3F1EA5 and #RG11916B8 7F55459) to EB; by Banca d'Italia funded grant (#1130944/22) to EB; PROGETTO PRIN funded by the Italian Ministry of University and Research #20223S7JKZ to EB and VB; Project AD-RIDDLE European Union in the HORIZON-JU-RIA Program, Contract #101132933 to PM; Fondazione Perugia 2023, #21928 to PM; Project LETHE European Union H2020 Program, Contract #101017405 to PM; Fondazione Cassa di Risparmio di Perugia #2019.0324.026FCRPG to PM; Italian Ministry of Health #PE-2016-02362694) to PM; Project RECAGE European Union H2020 Program, #779237 to PM.

## Declaration of competing interest

The authors declare that they have no competing interests.

## Acknowledgements

Not Applicable

## Appendix A. Supplementary data

Supplementary data to this article can be found online at https://doi.org/10.1016/j.nbd.2026.107291.

## Data availability

Data will be made available on request.

## References

Ables, J.L., Breunig, J.J., Eisch, A.J., Rakic, P., 2011. Not(ch) just development: notch signalling in the adult brain. Nat. Rev. Neurosci. 12 (5), 269–283.
Aluise, C.D., Robinson, R.A., Beckett, T.L., Murphy, M.P., Cai, J., Pierce, W.M., et al., 2010. Preclinical Alzheimer disease: brain oxidative stress, Abeta peptide and proteomics. Neurobiol. Dis. 39 (2), 221–228.
Aluise, C.D., Robinson, R.A., Cai, J., Pierce, W.M., Markesbery, W.R., Butterfield, D.A., 2011. Redox proteomics analysis of brains from subjects with amnestic mild cognitive impairment compared to brains from subjects with preclinical Alzheimer's disease: insights into memory loss in MCI. J. Alzheimer's Dis 23 (2), 257–269.
Annweiler, C., Duval, G.T., Cheng, C.Y., Wong, T.Y., Lamoureux, E.L., Milea, D., et al., 2019. U-shaped relationship between serum leptin concentration and cognitive performance in older Asian adults. Nutrients 11 (3).
Barone, E., Butterfield, D.A., 2025. Insulin signaling in microglia: a metabolic switch controlling neuroinflammation and amyloid pathology in Alzheimer's disease. Cell Metab. 37 (8), 1630–1632.
Boccardi, V., Travaglini, E.G., Sciacca, E., Mancinetti, F., Murasecco, I., Guazzarini, A.G., et al., 2024. Dysglycemia, gender, and cognitive performance in older persons living with mild cognitive impairment: findings from a cross-sectional, population-based study. Aging Clin. Exp. Res. 36 (1), 145.
Butterfield, D.A., Halliwell, B., 2019. Oxidative stress, dysfunctional glucose metabolism and Alzheimer disease. Nat. Rev. Neurosci. 20 (3), 148–160.
Castro-Aldrete, L., Einsiedler, M., Novakova Martinkova, J., Depypere, H., Alvin Ang, T. F., Mielke, M.M., et al., 2025. Alzheimer disease seen through the lens of sex and gender. Nat. Rev. Neurol. 21 (5), 235–249.
Charisis, S., Short, M.I., Bernal, R., Kautz, T.F., Trevino, H.A., Mathews, J., et al., 2024. Leptin bioavailability and markers of brain atrophy and vascular injury in the middle age. Alzheimers Dement. 20 (9), 5849–5860.
Chiariello, A., Valente, S., Pasquinelli, G., Baracca, A., Sgarbi, G., Solaini, G., et al., 2022. The expression pattern of GDF15 in human brain changes during aging and in Alzheimer's disease. Front. Aging Neurosci. 14, 1058665.
Conte, M., Giuliani, C., Chiariello, A., Iannuzzi, V., Franceschi, C., Salvioli, S., 2022. GDF15, an emerging key player in human aging. Ageing Res. Rev. 75, 101569.
Demetrius, L.A., Eckert, A., Grimm, A., 2021. Sex differences in Alzheimer's disease: metabolic reprogramming and therapeutic intervention. Trends Endocrinol. Metab. 32 (12), 963–979.
Folstein, M.F., Folstein, S.E., McHugh, P.R., 1975. "Mini-mental state". A practical method for grading the cognitive state of patients for the clinician. J. Psychiatr. Res. 12 (3), 189–198.
Franceschi, C., Garagnani, P., Parini, P., Giuliani, C., Santoro, A., 2018. Inflammaging: a new immune-metabolic viewpoint for age-related diseases. Nat. Rev. Endocrinol. 14 (10), 576–590.
Gauthier, S.A., Perez-Gonzalez, R., Sharma, A., Huang, F.K., Alldred, M.J., Pawlik, M., et al., 2017. Enhanced exosome secretion in Down syndrome brain - a protective mechanism to alleviate neuronal endosomal abnormalities. Acta Neuropathol. Commun. 5 (1), 65.
Huang, Y., Feng, J., Xu, J., Dong, L., Su, W., Li, B., et al., 2025. Associations of age and sex with characteristics of extracellular vesicles and protein-enriched fractions of blood plasma. Aging Cell 24 (1), e14356.
Huque, H., Eramudugolla, R., Chidiac, B., Ee, N., Ehrenfeld, L., Matthews, F.E., et al., 2023. Could country-level factors explain sex differences in dementia incidence and prevalence? A systematic review and Meta-analysis. J. Alzheimer's Dis 91 (4), 1231–1241.
Jack Jr., C.R., Arani, A., Borowski, B.J., Cash, D.M., Crawford, K., Das, S.R., et al., 2024. Overview of ADNI MRI. Alzheimers Dement. 20 (10), 7350–7360.
Jena, J., Garcia-Pena, L.M., Pereira, R.O., 2023. The roles of FGF21 and GDF15 in mediating the mitochondrial integrated stress response. Front. Endocrinol. (Lausanne) 14, 1264530.
Jiang, Q., Liu, J., Huang, S., Wang, X.Y., Chen, X., Liu, G.H., et al., 2025. Antiageing strategy for neurodegenerative diseases: from mechanisms to clinical advances. Signal Transduct. Target. Ther. 10 (1), 76.
Kapogiannis, D., Mustapic, M., Shardell, M.D., Berkowitz, S.T., Diehl, T.C., Spangler, R. D., et al., 2019. Association of extracellular vesicle biomarkers with Alzheimer disease in the Baltimore longitudinal study of aging. JAMA Neurol. 76 (11), 1340–1351.
Kapogiannis, D., Manolopoulos, A., Mullins, R., Avgerinos, K., Delgado-Peraza, F., Mustapic, M., et al., 2024. Brain responses to intermittent fasting and the healthy living diet in older adults. Cell Metab. 36 (8), 1668–78 e5.
Kapoor, A., Nation, D.A., 2021. Role of notch signaling in neurovascular aging and Alzheimer's disease. Semin. Cell Dev. Biol. 116, 90–97.
Katsimpardi, L., Litterman, N.K., Schein, P.A., Miller, C.M., Loffredo, F.S., Wojtkiewicz, G.R., et al., 2014. Vascular and neurogenic rejuvenation of the aging mouse brain by young systemic factors. Science 344 (6184), 630–634.
Katz, S., Ford, A.B., Moskowitz, R.W., Jackson, B.A., Jaffe, M.W., 1963. Studies of illness in the aged. The index of Adl: a standardized measure of biological and psychosocial function. JAMA 185, 914–919.
Keith, C.M., Haut, M.W., Vieira Ligo Teixeira, C., Mehta, R.I., Phelps, H., Ward, M., et al., 2024. Memory consolidation, temporal and parietal atrophy, and metabolism in amyloid-beta positive and negative mild cognitive impairment. J. Alzheimer's Dis 102 (3), 778–791.
Kim, Y., Pérez-González, R., Miller, C., Kurz, M., D'Acunzo, P., Goulbourne, C.N., et al., 2022. Sex differentially alters secretion of brain extracellular vesicles during aging: a potential mechanism for maintaining brain homeostasis. Neurochem. Res. 47 (11), 3428–3439.
Lampada, A., Taylor, V., 2023. Notch signaling as a master regulator of adult neurogenesis. Front. Neurosci. 17, 1179011.
Lawton, M.P., Brody, E.M., 1969. Assessment of older people: self-maintaining and instrumental activities of daily living. Gerontologist 9 (3), 179–186.
Ledreux, A., Carmona-Iragui, M., Videla, L., Benejam, B., Barroeta, I., Lleo, A., et al., 2025. Cargo of small extracellular vesicles from neuronal origin shows progression of dementia in individuals with Down syndrome. Alzheimers Dement. 21 (6), e70380.
Lieb, W., Beiser, A.S., Vasan, R.S., Tan, Z.S., Au, R., Harris, T.B., et al., 2009. Association of plasma leptin levels with incident Alzheimer disease and MRI measures of brain aging. JAMA 302 (23), 2565–2572.
Liu, H., Huang, Y., Lyu, Y., Dai, W., Tong, Y., Li, Y., 2021. GDF15 as a biomarker of ageing. Exp. Gerontol. 146, 111228.
Liu, W.S., You, J., Chen, S.D., Zhang, Y., Feng, J.F., Xu, Y.M., et al., 2025. Plasma proteomics identify biomarkers and undulating changes of brain aging. Nat. Aging 5 (1), 99–112.
Maioli, S., Lodeiro, M., Merino-Serrais, P., Falahati, F., Khan, W., Puerta, E., et al., 2015. Alterations in brain leptin signalling in spite of unchanged CSF leptin levels in Alzheimer's disease. Aging Cell 14 (1), 122–129.
Mancuso, C., Siciliano, R., Barone, E., 2011. Curcumin and Alzheimer disease: this marriage is not to be performed. J. Biol. Chem. 286 (3) (le3; author reply le4).
Manolopoulos, A., Delgado-Peraza, F., Mustapic, M., Pucha, K.A., Nogueras-Ortiz, C., Daskalopoulos, A., et al., 2023. Comparative assessment of Alzheimer's disease-related biomarkers in plasma and neuron-derived extracellular vesicles: a nested case-control study. Front. Mol. Biosci. 10, 1254834.
Manolopoulos, A., Yao, P.J., Kapogiannis, D., 2025. Extracellular vesicles: translational research and applications in neurology. Nat. Rev. Neurol. 21 (5), 265–282.
McKhann, G.M., Knopman, D.S., Chertkow, H., Hyman, B.T., Jack Jr., C.R., Kawas, C.H., et al., 2011. The diagnosis of dementia due to Alzheimer's disease: recommendations from the National Institute on Aging-Alzheimer's Association workgroups on diagnostic guidelines for Alzheimer's disease. Alzheimers Dement. 7 (3), 263–269.
Moqri, M., Herzog, C., Poganik, J.R., Biomarkers of Aging C, Justice, J., Belsky, D.W., et al., 2023. Biomarkers of aging for the identification and evaluation of longevity interventions. Cell 186 (18), 3758–3775.
Muehlboeck, J.S., Westman, E., Simmons, A., 2014. TheHiveDB image data management and analysis framework. Front. Neuroinform. 7, 49.
Muller, L., Di Benedetto, S., 2025. Neuroimmune crosstalk in chronic neuroinflammation: microglial interactions and immune modulation. Front. Cell. Neurosci. 19, 1575022.
Mustapic, M., Eitan, E., Werner Jr., J.K., Berkowitz, S.T., Lazaropoulos, M.P., Tran, J., et al., 2017. Plasma extracellular vesicles enriched for neuronal origin: a potential window into brain pathologic processes. Front. Neurosci. 11, 278.
Nakamichi, A., Kimura, N., Hanaoka, T., Masuda, T., Ataka, T., Matsubara, E., 2025. Association between plasma cytokine levels and multiple neuroimaging modalities in mild cognitive impairment. J. Alzheimer's Dis 104 (1), 129–137.

Nogueras-Ortiz, C.J., Eren, E., Yao, P., Calzada, E., Dunn, C., Volpert, O., et al., 2024. Single-extracellular vesicle (EV) analyses validate the use of L1 cell adhesion molecule (L1CAM) as a reliable biomarker of neuron-derived EVs. J. Extracell. Vesicles 13 (6), e12459.
Noren Hooten, N., Byappanahalli, A.M., Vannoy, M., Omoniyi, V., Evans, M.K., 2022. Influences of age, race, and sex on extracellular vesicle characteristics. Theranostics 12 (9), 4459–4476.
Ormazabal, P., Bastias-Perez, M., Inestrosa, N.C., Cisternas, P., 2025. Adipokines at the metabolic-brain interface: therapeutic modulation by antidiabetic agents and natural compounds in Alzheimer's disease. Pharmaceuticals (Basel) 18 (10).
Oveisgharan, S., Arvanitakis, Z., Yu, L., Farfel, J., Schneider, J.A., Bennett, D.A., 2018. Sex differences in Alzheimer's disease and common neuropathologies of aging. Acta Neuropathol. 136 (6), 887–900.
Peng, K.Y., Pérez-González, R., Alldred, M.J., Goulbourne, C.N., Morales-Corraliza, J., Saito, M., et al., 2019. Apolipoprotein E4 genotype compromises brain exosome production. Brain 142 (1), 163–175.
Perluigi, M., Picca, A., Montanari, E., Calvani, R., Marini, F., Matassa, R., et al., 2022. Aberrant crosstalk between insulin signaling and mTOR in young Down syndrome individuals revealed by neuronal-derived extracellular vesicles. Alzheimers Dement. 18 (8), 1498–1510.
Perluigi, M., Di Domenico, F., Butterfield, D.A., 2024. Oxidative damage in neurodegeneration: roles in the pathogenesis and progression of Alzheimer disease. Physiol. Rev. 104 (1), 103–197.
Rajan, K.B., Weuve, J., Barnes, L.L., McAninch, E.A., Wilson, R.S., Evans, D.A., 2021. Population estimate of people with clinical Alzheimer's disease and mild cognitive impairment in the United States (2020-2060). Alzheimers Dement. 17 (12), 1966–1975.
Thery, C., Witwer, K.W., Aikawa, E., Alcaraz, M.J., Anderson, J.D., Andriantsitohaina, R., et al., 2018. Minimal information for studies of extracellular vesicles 2018 (MISEV2018): a position statement of the International Society for Extracellular Vesicles and update of the MISEV2014 guidelines. J. Extracell. Vesicles 7 (1), 1535750.
Tian, L., Ma, L., Kaarela, T., Li, Z., 2012. Neuroimmune crosstalk in the central nervous system and its significance for neurological diseases. J. Neuroinflammation 9, 155.
Tramutola, A., Sharma, N., Barone, E., Lanzillotta, C., Castellani, A., Iavarone, F., et al., 2018. Proteomic identification of altered protein O-GlcNAcylation in a triple transgenic mouse model of Alzheimer's disease. Biochim. Biophys. Acta Mol. basis Dis. 1864 (10), 3309–3321.
Triani, F., Tramutola, A., Di Domenico, F., Sharma, N., Butterfield, D.A., Head, E., et al., 2018. Biliverdin reductase-A impairment links brain insulin resistance with increased Abeta production in an animal model of aging: implications for Alzheimer disease. Biochim. Biophys. Acta Mol. basis Dis. 1864 (10), 3181–3194.
Wang, D.X., Dong, Z.J., Deng, S.X., Tian, Y.M., Xiao, Y.J., Li, X., et al., 2023. GDF11 slows excitatory neuronal senescence and brain ageing by repressing p21. Nat. Commun. 14 (1), 7476.
Welsh, J.A., Goberdhan, D.C.I., O'Driscoll, L., Buzas, E.I., Blenkiron, C., Bussolati, B., et al., 2024. Minimal information for studies of extracellular vesicles (MISEV2023): from basic to advanced approaches. J. Extracell. Vesicles 13 (2), e12404.
Wen, S., Wang, J., Liu, W., Meng, X., Jiao, Z., 2025a. Spatio-temporal dynamic functional brain network for mild cognitive impairment analysis. Front. Neurosci. 19, 1597777.
Wen, H., Deng, H., Li, B., Chen, J., Zhu, J., Zhang, X., et al., 2025b. Mitochondrial diseases: from molecular mechanisms to therapeutic advances. Signal Transduct. Target. Ther. 10 (1), 9.
Zhang, J., Zhang, Y., Wang, J., Xia, Y., Zhang, J., Chen, L., 2024. Recent advances in Alzheimer's disease: mechanisms, clinical trials and new drug development strategies. Signal Transduct. Target. Ther. 9 (1), 211.